Quarterly Report for
**October - December 2000
Stanford Geothermal Program**
DE-FG07-99ID13763

Table of Contents

1. MEASUREMENTS OF STEAM-WATER RELATIVE PERMEABILITY

This research project is being conducted by Research Assistant Peter O'Connor and Professor Roland Horne. The aim is to measure relative permeability relations for steam and water flowing simultaneously in rock and to examine the effects of temperature, flow rate, and rock type. The experiment will attempt to reproduce results obtained in a previous experiment (Mahiya, 1999), but holding the experimental pressure as close as possible to a constant value.

1.1 BACKGROUND

An X-ray CT technique has been used in recent years to measure the distribution of steam and water saturation in rocks to obtain steam-water relative permeability curves (Satik and Horne, 1998, Mahiya, 1999).

The current experiment is attempting to maintain a constant pressure, to avoid complications of the slip factor. As the experiment will be constantly at an inlet gauge pressure of 15 psi, it will necessarily be at a constant 120ºC at the inlet in order to have two-phase flow throughout, with the rest of the core being at the saturation temperature for the pressure at that point. Our expectation is an identical pressure profile and temperature profile for every step of the process.

1.2 EXPERIMENTAL PROCEDURE

A Berea sandstone will be drained, flushed with nitrogen, then subjected to a vacuum. A dry X-ray scan is then made to obtain CT_{dry}. The core is saturated with water and scanned to obtain CT_{wet}; from these scans, a porosity distribution will be obtained, expected to yield an average value of 24.7%. In the next step, hot liquid water is flowed through to obtain CT_{hw}, which is necessary to calculate experimental saturations. The next steps are to reproduce the actual flow-through experiments, at rates which have already been established by simulation and advance experimentation. The core will be under a pressure gradient of approximately 15 psi across the 41-cm length. First, the core is saturated with steam. Steam flow rate will be lowered gradually in ~10% increments, to implement an imbibition process whereby the wetting phase (water) displaces the nonwetting phase (steam). A flexible heat guard ensures negligible overall heat loss for a near-adiabatic process. The flexible heat guard control mechanism was redesigned this year. At each step, the system will reach a steady state and will then be subject to CT scan to measure saturation. Steam flow rate will be reduced to 0%, then increased. This second sequence will be a drainage sequence.

At every stage, pressure, temperature and heat fluxes from the core are to be measured. Calculated relative permeability to steam and water are then plotted against the saturation measurements. The major suggested change from the previous experiment is to perform the imbibition step first. Performing the imbibition step first allows determination of the maximum pressure. This pressure can be maintained by increasing flow rates if necessary.
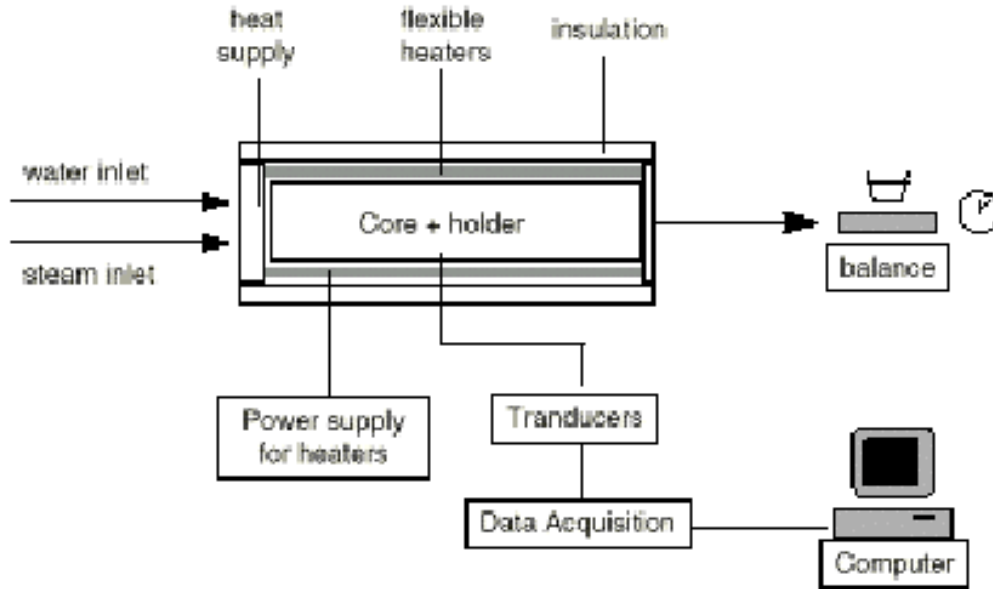
Figure 1.1: Experimental apparatus for relative permeability measurement.

1.4 EXPERIMENTAL PROGRESS

During the current quarter, we worked with the apparatus depicted in Figure 1.1 to determine the correct flow rates and power inputs to ensure a pressure differential of 15 psi and a temperature at the inlet of slightly over 120ºC for the steam, and slightly under 120ºC for the hot water. Early in the quarter, the end piece containing the steam and water inlets failed. We have since replaced it with a stainless steel end piece that includes a thermal switch, preventing any high-temperature failure. Subsequently, we have determined a complete set of flow rates for water and steam, at different ratios, to result in steady-state flow with a pressure differential of 15 psi. This process also determined the corresponding voltage and current settings for the hot water and steam heaters and for the flexible heater. All that is unknown is the saturation; CT scanning is to begin early in the winter quarter, to determine the saturation.

The steel end piece presents some challenges that the plastic one did not; there appears to be greater heat flow between the fluid heaters. It is hoped that this heat flow is moderate enough that we still have single-phase flow coming from each inlet, and we are adjusting the settings to compensate.

1.5 FUTURE RESEARCH

Future research will involve repeating the experiment at different pressure gradients and temperatures. The next experiment will probably occur at approximately half the current pressure gradient. In each case, the experiment will maintain a uniform pressure gradient

for the range of saturations. The current apparatus is not likely be suitable for conducting a similar experiment at significantly higher pressure gradients or temperature.

Also under consideration are other possible methods of measuring saturation, either by weighing the core or using acoustic sounding to determine saturation. While not as precise as the CT scanner, these methods have the advantage of producing average saturation readings extremely quickly.

Basic calculations show that a water-saturated core at 120ºC would weigh 0.2 kg more than a steam-saturated core. Such a difference is great enough to allow for measurement of the whole range of saturations; however, it would require the assumption of uniform saturation throughout the core. The presence of a steam front would not be detected by simply weighing the core. In this case, we could use an end-to-end acoustic signal to detect the presence of a wave front. The sound speed through an air-water mixture is considerably less than the sound speed through either air or water (Gudmundsson, 1992), and it is expected that this relation holds true for a steam-water mixture as well. Thus, the presence of a wave front would produce a reflected signal.

In theory, acoustic sounding could be used to determine not only the location of the wave front but even the saturation of the core. Several sensors could be placed, to determine saturations at many locations simultaneously. Saturation-sound speed relations could be calculated theoretically using either the Gassman or Hashin-Shtrikman relations or could be calibrated using the CT scanner. However, Gudmundsson's 1992 results appear to indicate this method would be impractical; the sound speed is nearly constant across most two-phase regions. It is only at very high or very low water saturation that the sound speed differs by more than the margin of error.

2. STEAM-WATER CAPILLARY PRESSURE

This project is being conducted by Research Associate Kewen Li and Professor Roland Horne. The objective is to develop a method to calculate steam-water capillary pressure and relative permeability from spontaneous water imbibition data. In this report, we present the experimental results of capillary pressure from both the water imbibition and the X-ray CT methods.

2.1 SUMMARY

We conducted spontaneous water imbibition in a core sample and calculated the capillary pressure using the method that we developed previously. Then we measured the air-water capillary pressure using an X-ray CT technique and compared the results with those calculated from water imbibition data. It was found that the results of capillary pressure measured using the two different methods were consistent. This confirmed that the method that we developed to calculate capillary pressure from the water imbibition data is valid.

2.2 INTRODUCTION

An analytical method was developed by Li and Horne (2000) to calculate capillary pressure from the spontaneous water imbibition data and had been confirmed by experiments in an unconsolidated glass-bead pack but not in a consolidated porous medium. Therefore in this stage of the study, we conducted spontaneous water imbibition in a consolidated ceramic core and obtained the results of the capillary pressure using two different methods.

2.3 THEORY

The process of spontaneous water imbibition into a gas-saturated core can be characterized as follows (Li and Horne, 2000):

$$Q_w = \frac{dN_{wt}}{dt} = a\frac{1}{\eta} - b \tag{2.1}$$

where:

$$a = \frac{Ak_w(S_{wf} - S_{wi})}{\mu_w L}P_c \tag{2.2}$$

$$b = \frac{Ak_w}{\mu_w}\Delta\rho g \tag{2.3}$$

and:

$$\eta = \frac{N_{wt}}{V_p} \tag{2.4}$$

where A and N_{wt} are the cross-section area of the core and the volume of water imbibed into the core; μ_w is the viscosity of water and t is the imbibition time; S_{wi} is the initial water saturation before water imbibition; S_{wf} is the water saturation behind the imbibition front; k_w is the effective permeability of water phase at a water saturation of S_{wf}; P_c is the capillary pressure at S_{wf}; $\Delta\rho$ is the density difference between gas and liquid; g is gravity constant; L and V_p are the core length and the pore volume of the core sample; η is the gas recovery by water imbibition in terms of pore volume.

Based on Eqs. 2.2 and 2.3, capillary pressure can be calculated:

$$P_c = \frac{1}{(S_{wf} - S_{wi})} \frac{a}{b} \Delta\rho g L \qquad (2.5)$$

The values of a and b in Eq. 2.5 can be calculated from the plot of imbibition rate and the reciprocal of the gas recovery. S_{wf} can be measured during the water imbibition test. Therefore, we can compute capillary pressure using Eq. 2.5.

According to Eq. 2.3, the effective water permeability at the water saturation of S_{wf} can be computed as follows:

$$k_w = \frac{\mu_w}{A\Delta\rho g} b \qquad (2.6)$$

2.4 EXPERIMENTS

Rock and Fluids. Distilled water was used as the liquid phase; the specific gravity and viscosity were 1.0 and 1.0 cp at 20ºC. Steam and air were used as the gas phase; the surface tension of water/air at 20ºC was 72.75 dynes/cm. The ceramic sample was provided by Refractron Technologies Corp. It had a porosity of 39.19%, a length of 25.0 cm, an inner diameter of 4.275 cm and an outer diameter of 6.287 cm. We did not measure the permeability of the core sample yet due to its special shape but the permeability was estimated to be over 10 darcy.

X-ray CT Scanner. Distribution of water saturation in the core sample was measured using a Picker[TM] Synerview X-ray CT scanner (Model 1200 SX) with 1200 fixed detectors. The voxel dimension was 0.5 mm by 0.5 mm by 5 mm, the tube current used was 50 mA, and the energy level of the radiation was 140 keV. The acquisition time of one image was about 3 seconds while the processing time was around 40 seconds.

Apparatus. A schematic of the apparatus to conduct water imbibition tests in air-saturated porous media is shown in Figure 2.1. The core sample was hung under a Mettler balance (Model PE 1600) which had an accuracy of 0.01g and a range from 0 to 1600 g. The water imbibed into the core sample was recorded in time by the balance using an under-weighing method and the data were measured continuously by a computer

through an RS-232 interface. The purpose of using the under-weighing method is to reduce the experimental error caused by water evaporation.
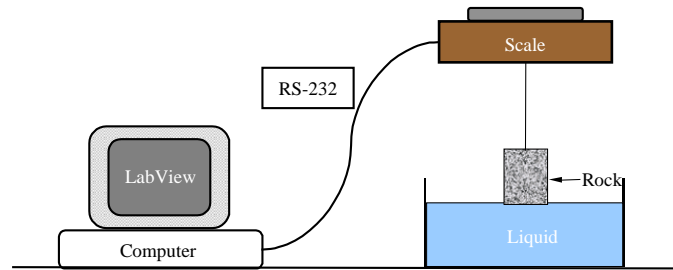
Figure 2.1: Schematic of apparatus for imbibition test.

The sample was not in contact with the water until the imbibition tests began. The water level in the container could be adjusted by raising or lowering the container using an adjustable jack.

Procedure. The samples were dried by heating to a temperature of 105ºC until their weight did not vary during eight hours or more. The core was assembled in the apparatus after it was cooled down, as shown in Figure 2.1. Water started to imbibe into the core once the bottom of the sample was brought in contact with the water surface by raising the water container. The weight change of the core sample was then recorded in time and used to calculate the effective permeability of water phase and the capillary pressure.

The core was positioned vertically in the experiment. An X-ray CT scan was made at each centimeter along the sample before and after the water imbibition test. Finally, the sample was dried and another X-ray CT scan was made after completely resaturating with water. The CT values measured under three different states were used to calculate the porosity and the distribution of the water saturation as a function of height.

2.5 RESULTS

Figure 2.2 plots the amount of water imbibition into the core as a function of time. The water imbibition test lasted about 2000 minutes. Figure 2.3 shows that the relationship between the water imbibition rate and the reciprocal of the gas recovery is linear over a certain period of the imbibition process, as prescribed by the theory developed by Li and Horne (2000). The linearity implies that the water imbibition front may be piston-like as was assumed. Another important feature shown in Figure 2.3 is that the straight line does not go through the origin, as foreseen by Eq. 2.1. This feature demonstrates that the effect of the gravity force cannot be neglected.
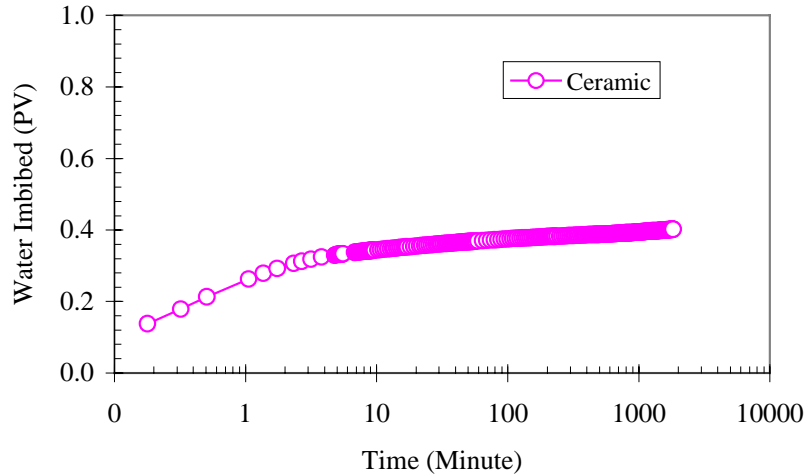
Figure 2.2: Water imbibition vs. time in the ceramic core.
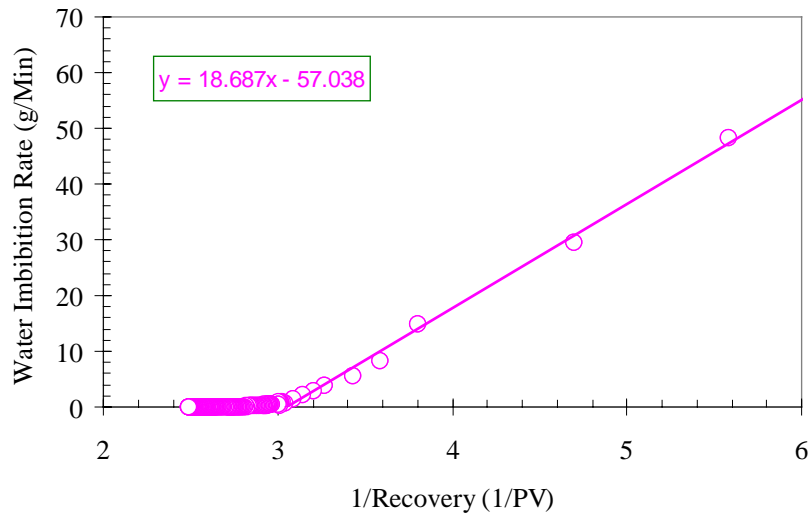
Figure 2.3: Water imbibition rate vs. the reciprocal of the gas recovery in the core.

When the imbibition front reached a certain height in the core, the imbibition process may not be a capillary pressure-dominated process as we assumed in the mathematical derivation. The reason is that the effect of the gravity on the imbibition process increases with the height of the imbibition front. The water imbibition mechanism may transfer from piston-like to diffusion-type. Eq. 2.1 is not appropriate to diffusion-type imbibition. This may explain why the relationship between the water imbibition rate and the reciprocal of production in the core shifts from the main trend at late time as shown in Figure 2.3.

The relationship between the water gain and the square root of imbibition time in the core is shown in Figure 2.4. The time interval in Figure 2.4 is about the same as that corresponding to the linear section of the relationship in Figure 2.3. There is no linear

correlation between the amount of water imbibed and the square root of imbibition time for the same time interval, as suggested by the Handy function.
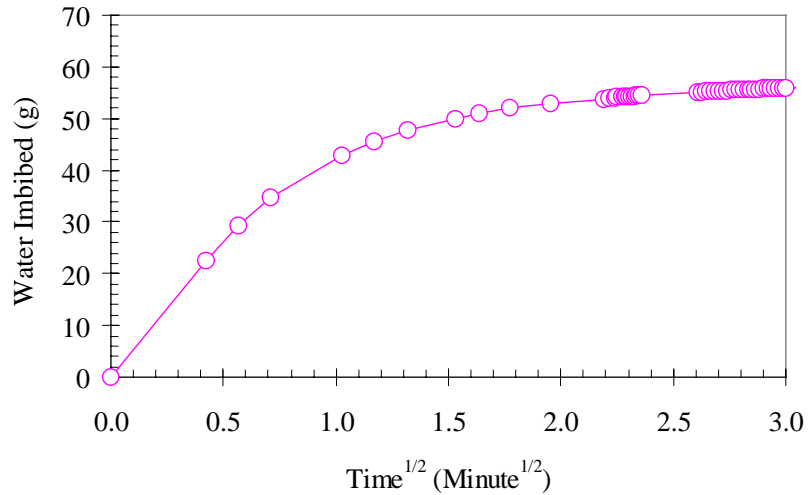
Figure 2.4: Water imbibition vs. the square root of time in the core.

The imbibition capillary pressure at the water saturation behind the imbibition front calculated using Eq. 2.5 and the data shown in Figure 2.2 is 9.98 cm (water column). We will compare this value to the capillary pressure measured in the core using the X-ray CT technique.

The distribution of the porosity of the core from the bottom to the top was measured using the X-ray CT technique, and is shown in Figure 2.5. The porosity distribution along the height of this ceramic core sample was homogeneous. The average porosity from Figure 2.5 was 39.61%. The porosity measured by weighing the core sample before and after saturating with water was 39.19%, which was in good agreement. Note that the core used in this study had a hollow center. So the method to calculate porosity using CT values was different from the one we use normally. The details of this modified procedure were discussed by Li and Horne (2001).
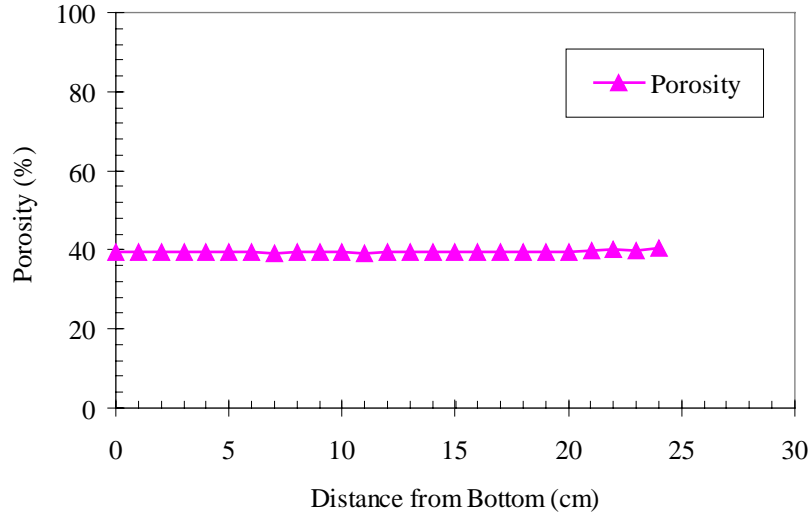
Figure 2.5: Porosity distribution in the core.

The distribution of CT values before and after the water imbibition test is shown in Figure 2.6. CT_{dry} in this figure represents the CT value of the core when it is air-saturated and CT_{obj} represents the CT value after the water imbibition was finished.

It was assumed that the balance between the gravity force and the capillarity force was reached after the water imbibition was finished. Therefore, the capillary pressure at any position in the core was equal to the gravity force at the same position, which is the water column height at this point. The corresponding water saturation at this position was measured using the X-ray CT technique. The air-water imbibition capillary pressure curve measured using this method is plotted in Figure 2.7. We can see in Figure 2.7 that the air-water capillary pressure at the water saturation behind the imbibition front (actually the maximum water saturation), $P_c(S_{wf})$, is about 9 cm (water column). Therefore, the capillary pressure calculated using Eq. 2.5 is approximately equal to that measured using the X-ray CT method at the same water saturation of S_{wf}. This consistency demonstrated the validity of the method we developed earlier to calculate the capillary pressure using spontaneous water imbibition data, for this new case of a consolidated porous medium.

9
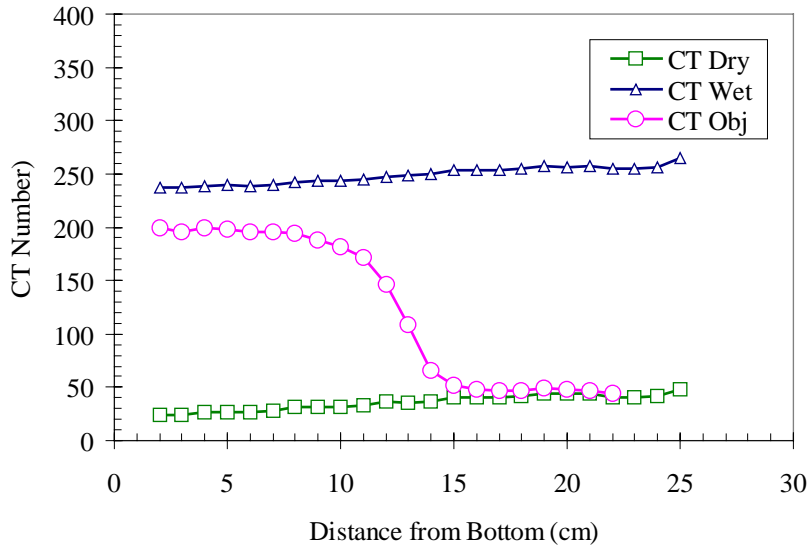
Figure2.6: Distribution of CT values before and after imbibition test.
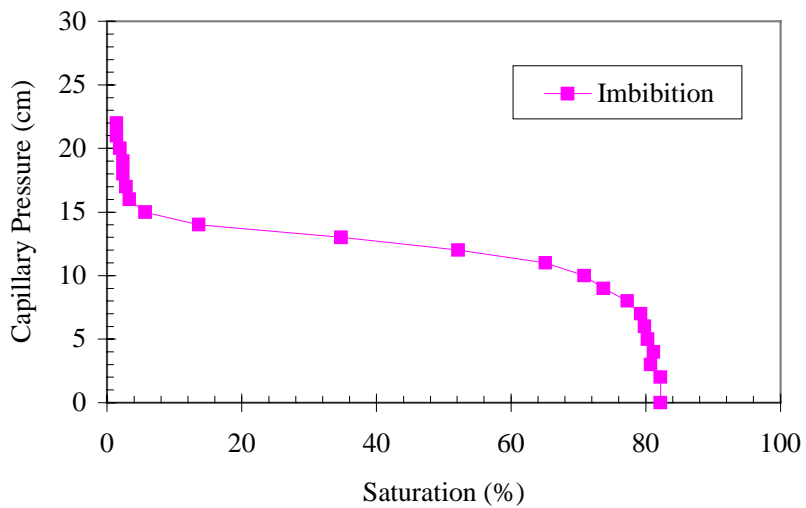
Figure 2.7: Air-water imbibition capillary pressure of the core.

2.6 CONCLUSIONS

Based on the present work, the following conclusions may be drawn:
1. The relationship between the water imbibition rate and the reciprocal of the gas recovery is linear in the core we studied.
2. The capillary pressure calculated using the water imbibition data was nearly equal to that measured by the X-ray CT technique.

2.7 FUTURE WORK

We plan to conduct water imbibition in steam-saturated rocks.

3. GAS SLIPPAGE IN STEAM-WATER TWO-PHASE FLOW

This project is being conducted by Research Associate Kewen Li and Professor Roland Horne. In this study gas slip factors in gas-water two-phase flow were measured. The effects of temperature on both nitrogen and steam slip factors were also investigated in order to calibrate steam-phase relative permeabilities. This stage of the project was concluded this quarter and a scientific paper describing the results was prepared for publication.

3.1 SUMMARY

Gas slippage (the Klinkenberg effect) in single-phase gas flow has been investigated extensively. However, few papers have been published on gas slippage in gas-liquid two-phase flow. The gas relative permeabilities at water saturations close to the residual value have been found to be significantly greater than one in both nitrogen-water and steam-water flow through rocks. These values became less than one after the calculation was calibrated by taking the two-phase gas slip effect into consideration (Mahiya, 1999). The gas relative permeabilities have been measured at different mean pore pressures and the values of two-phase gas slip factor have been computed at different water saturations. The effects of temperature on both nitrogen and steam slip factors have also been studied and compared. These data have then been used to conduct a calibration in order to obtain intrinsic gas relative permeabilities that do not vary with the test pressures. It has been found from the present work that neglecting the two-phase gas slip effect may overestimate gas relative permeabilities. It is the intrinsic gas relative permeabilities instead of those measured at low test pressure that should be utilized in numerical simulation or other reservoir engineering calculations.

3.2 INTRODUCTION

Gas-liquid relative permeabilities are fundamental properties in reservoir engineering and numerical simulation. There may be significant effect of gas slippage in gas-liquid two-phase flow. However, few experimental data regarding the gas slip effect in two-phase flow have been published. If the slip effect is not considered correctly, the gas relative permeabilities will vary with test pressures and may be greater than one at some water saturations. On the other hand, little attention has been paid to the measurements of steam slip factor even in single-phase flow. Reliable data for steam flow is essential to the study of steam injection in heavy oil reservoirs or water injection in geothermal reservoirs where steam is produced.

Rose (1948) conducted experimental measurements of gas relative permeabilities in both synthetic cores (Alundum filters) and natural sandstone cores. Rose (1948) reported that the gas slip factor of the sandstone cores decreased with the increase of the liquid (water) saturation. Fulton (1951) performed experiments on Pyrex cylindrical filters and also found that the gas slip factor decreased with the increase of the liquid (water) saturation in a range from 0 to about 30%. These experiments were not conducted at liquid saturations above 30%. Therefore, Estes and Fulton (1956) extended their experiments to liquid saturations over 30%, ranging from 0 to about 88% using Soltrol oil as the liquid

phase; they found a similar phenomenon to that described by Rose (1948) and Fulton (1951).

Although many researchers, including Sampath and Keighin (1982), demonstrated the decrease of gas slip factor with the increase of liquid saturation, the reason for which is not readily apparent. Actually, the experimental data presented by these authors are contradictory to the Klinkenberg (1941) equation, which is expressed as follows:

$$k_g = k_{g\infty}(1 + \frac{4c\lambda}{r})$$ (3.1)

where k_g is the gas permeability at a mean pressure, p_m, and $k_{g\infty}$ the intrinsic permeability of gas at an infinite pressure; c is a proportionality factor with an apparent value of slightly less than 1; λ is the mean free path of the gas and r the average radius of the capillaries.

As the mean free path of the gas is inversely proportional to the mean pressure, p_m, Klinkenberg (1941) reduced Eq. 3.1 as follows:

$$k_g = k_{g\infty}(1 + \frac{b}{p_m})$$ (3.2)

where p_m is the mean pressure which is defined by $p_m = (p_i + p_o)/2$; p_i and p_o are the inlet and outlet pressures of the cores, respectively. b is the gas slip factor, which is defined as:

$$b = \frac{4c}{r}\frac{\lambda}{p_m}$$ (3.3)

Since λ/p_m is a constant, Eq. 3.3 can be reduced as follows:

$$b = \frac{4c'}{r}$$ (3.4)

where c' is also constant.

Eq. 3.4 implies that the gas slip factor is inversely proportional to the radius of the capillaries. However, the effective radius of the capillaries (for gas phase) in porous media must be decreased with an increase in liquid saturation. Therefore, the gas slip factor should increase with the increase of the liquid saturation. Rose (1948) and Fulton (1951) gave different explanations to the contradiction between their data and the Klinkenberg theory.

In addition, Estes and Fulton (1956) found negative values of the gas slip factor at high liquid saturations in the vicinity of 65-75% for all of the natural cores they used. The negative value of b means that the apparent gas permeabilities measured at low pressures are smaller than those measured at high pressures. This, of course, is also contradictory to the Klinkenberg theory.

The common problems that existed in the studies of these researchers (Rose, 1948; Estes and Fulton, 1956) were the small size of the cores and the methods to establish the liquid saturations. The end effect due to the capillary discontinuity might have significant effect on the distribution of the liquid saturation in small cores.

Rose (1948) established the liquid saturations by a slow evaporation process. Fulton (1951) used two methods to obtain the desired water saturations; one was the same as Rose (1948) and the other one was by allowing the cores to imbibe water. Estes and Fulton (1956) achieved the liquid (oil) saturation either by allowing the oil to evaporate slowly from the cores or more frequently by removing the oil in increments with an absorbing tissue. Apparently, the distributions of the liquid saturations established using these methods would not be uniform. The nonuniform distribution of liquid saturation in the cores may affect the measurements of gas relative permeabilities. On the other hand, it is difficult to measure gas relative permeabilities at high liquid saturations, for example, above 50%, by allowing only gas to flow while keeping water immobile.

Jones and Owens (1980) measured the gas permeabilities on more than 100 tight gas sand samples with permeabilities ranging from 0.0001 to 1.0 md and their data yielded a relationship between b and $k_{g\infty}$ for single-phase gas flow:

$$b = 0.86 k_{g\infty}^{-0.33} \tag{3.5}$$

Sampath and Keighin (1982) thought that a correlation, if it exists, should be between b and $k_{g\infty}/\phi$ rather than between b and $k_{g\infty}$; they suggested a correlation between the gas slip factor and the intrinsic gas permeabilities based on their experimental results using nitrogen:

$$b = 0.0955(\frac{k_{g\infty}}{\phi})^{-0.53} \tag{3.6}$$

where ϕ is the porosity of the core sample.

Steam-water relative permeability is of importance in reservoir engineering for water injection into geothermal reservoirs. There are few measurements of steam-water relative permeabilities reported in the literature, and the values are frequently inconsistent. The main difficulties in making steam-water relative permeability measurements arise from the following aspects: (1) significant mass transfer between phases makes it difficult to measure or calculate fractional flow; (2) difficulties in measuring heat loss during

experiments; (3) unclear mechanisms of gas-liquid flow. For example, the effect of gas slippage on steam relative permeabilities in steam-water flow is not clear; very few studies related to the gas slip effect in steam-water flow have been published.

Satik and Horne (1998) observed an unusual phenomenon in that the values of steam relative permeability (k_{rg}), at some water saturations sometimes appear to be greater than one. A similar phenomenon was also found in experiments by Mahiya (1999). Steam is subject to a prominent flow characteristic of gas molecules: gas slippage. Gas permeability k_g at a low mean pressure is greater than the absolute liquid permeability (k) due to the gas slip effect. If the gas slippage is large enough, the gas permeability at low water saturation may still be greater than the absolute permeability. From the definition of relative permeability, k_g/k, the value of gas relative permeability may be greater than one. Hence the phenomenon of gas slippage may be the reason.

Counsil (1979) discussed gas slip effect and showed that the effect of gas slippage was small when $b = 0.2$ atm and $p_m = 10$ atm. So the gas (steam) slip effect was not considered in the analysis of the gas flow data. Counsil (1979) stated that "For the case of steam-water relative permeabilities, slip could be reduced by running experiments at very high pressures, and therefore very high temperatures". There are certain difficulties in running experiments at very high pressures and temperatures for measuring steam-water relative permeabilities, for example, when the X-ray CT method is used to measure the water saturation in a core (Ambusso *et al*., 1996). On the other hand, increasing experimental temperature will increase the value of b significantly as reported by Wel *et al*. (1986). An increasing b will increase the influence of gas slippage on steam flow properties.

Geothermal rock often has a very low intrinsic permeability of the order of 10^{-6} md. The value of b computed using Eq. 3.5 would be about 82.1 atm for this permeability. Thus the mean pressure would need to be about 1000 atm in order for the gas slip effect to be negligible in single-phase gas flow. Obviously, it is not easy to operate experiments at pressures over 1000 atm. It can be seen from this simple calculation that the effect of gas slippage on steam flow properties may be significant both in experiments as well as in actual geothermal reservoirs.

Herkelrath *et al*. (1983) recognized the importance of gas slippage and incorporated it into a single-phase steam flow model in order to model steam pressure-transient experimental data. In their study, the steam slip factor was substituted by the gas slip factor measured using nitrogen. There may be significant differences between steam and nitrogen slip factors as we found in this study.

In this study, gas-liquid relative permeabilities were measured at different pressures using an on-line weighing method with two balances. The effect of water saturation on the slip factor of nitrogen was investigated. A procedure of measuring and correcting gas (both nitrogen and steam) relative permeabilities was proposed. The slip factors of both nitrogen and steam were measured at different temperatures and compared. The

experimental values were used to correct the nitrogen and steam phase relative permeabilities.

3.3 THEORY

Assuming that Darcy's equation is valid for both nitrogen-water and steam-water two-phase flow and that capillary pressures are neglected, the effective permeability of gas phase (nitrogen and steam) is calculated using the following equation:

$$k_g(S_w, p_m) = \frac{q_g \mu_g L}{A \Delta p} \frac{p_o}{p_m}$$
(3.7)

where $k_g(S_w, p_m)$ is the effective gas phase permeability at a water saturation of S_w and a mean pressure of p_m; q_g and μ_g are the flow rate and viscosity of gas phase; Δp is the differential pressure across the core sample; A and L are the cross-section area and the length of the core sample. In Eq. 3.7, it is considered that gas permeability is not only a function of water saturation but also a function of mean pressure due to the gas slip effect.

The relative permeability of gas phase is usually calculated without the correction of gas slip effect as follows:

$$k_{rg}(S_w, p_m) = \frac{k_g(S_w, p_m)}{k}$$
(3.8)

where $k_{rg}(S_w, p_m)$ is the relative permeability of gas phase at a water saturation of S_w and a mean pressure of p_m; k is the absolute permeability of the rock sample measured by liquid injection.

With consideration of the gas slip effect, the intrinsic effective permeability of the gas phase, which is independent of mean pressure, is calculated using the following formula:

$$k_{g\infty}(S_w) = \frac{k_g(S_w, p_m)}{(1 + b_{S_w} / p_m)}$$
(3.9)

where $k_{g\infty}(S_w)$ and b_{Sw} are the intrinsic effective permeability and the slip factor of gas phase at a water saturation of S_w. Hence the relative permeability of gas phase with gas slip effect included is calculated using the following equation:

$$k_{rg\infty}(S_w) = \frac{k_{g\infty}(S_w)}{k}$$
(3.10)

where $k_{rg\infty}(S_w)$ is independent of test pressure and is named the intrinsic relative permeability of gas phase at a water saturation of S_w. It is seen from Eq. 3.9 that the

essential issue of calculating the intrinsic relative permeability of gas phase is to measure the value of b_{Sw}, the slip factor of gas phase at a water saturation of S_w.

Once the intrinsic gas relative permeabilities and the gas slip factors at different water saturations are available, the gas relative permeabilities at any mean pressure, $k_{rg}(S_w, p_m)$, can be computed as follows:

$$k_{rg}(S_w, p_m) = k_{rg\infty}(S_w)(1 + \frac{b_{S_w}}{p_m}) \tag{3.11}$$

Rose (1948) defined gas relative permeability differently as follows:

$$k'_{rg}(S_w, p_m) = \frac{k_g(S_w, p_m)}{k_g(S_w = 0, p_m)} \tag{3.12}$$

Substituting Eqs. 3.2 and 9 into Eq. 3.12:

$$k'_{rg}(S_w, p_m) = k_{rg\infty}(S_w)(\frac{1 + \dfrac{b_{S_w}}{p_m}}{1 + \dfrac{b}{p_m}}) \tag{3.13}$$

It is known from Eq. 3.13 that $k'_{rg}(S_w, p_m)$ would be close to $k_{rg\infty}(S_w)$ if the slip factor does not change with water saturation, as Rose (1948) reported. Given that $p_m = 1$ atm in Eq. 3.12, Eq. 3.13 can be reduced as follows:

$$k'_{rg}(S_w, p_m = 1) = k_{rg\infty}(S_w)(\frac{1 + b_{S_w}}{1 + b}) \tag{3.14}$$

where $k'_{rg}(S_w, p_m = 1)$ was the gas relative permeability defined by Estes and Fulton (1956).

Similarly, Eq. 3.14 states that $k'_{rg}(S_w, p_m = 1)$ would be close to $k_{rg\infty}(S_w)$ if the slip factor does not vary with water saturation, as Estes and Fulton (1956) reported. However, this may not be true for other cases. For example, our experimental data in this study showed that $k_{rg\infty}(S_w=24.1\%) = 0.693$ but $k'_{rg}(S_w = 24.1\%, p_m = 1) = 0.862$. Therefore, we defined the gas relative permeability using the usual way (see Eq. 3.8) and deployed $k_{rg\infty}(S_w)$ as the intrinsic gas relative permeability which is independent of mean pressure.

A steady-state method as illustrated in Figure 3.1 was used to measure the relative permeabilities of nitrogen-water, from which gas phase relative permeabilities were calculated using the methods described by Eqs. 3.8 to 3.10. Water phase relative

permeabilities can be calculated directly using Darcy's equation. The corresponding water saturations were calculated using either of the two balances in the apparatus (see Figure 3.1):

$$S_{w,i+1} = S_{w,i} - \frac{\Delta M_{i1}}{V_p \rho_w}, \quad \text{(using Balance 1)} \tag{3.15}$$

or

$$S_{w,i+1} = S_{w,i} + \frac{\Delta M_{i2}}{V_p \rho_w}, \quad \text{(using Balance 2)} \tag{3.16}$$

where V_p is the pore volume of the core sample; $S_{w,i}$ and $S_{w,i+1}$ are the water saturations at i^{th} and $i+1^{th}$ points, respectively; ΔM_{i1} and ΔM_{i2} are the weight variations recorded by Balances 1 and 2, respectively; ρ_w is the water density.

3.4 EXPERIMENTS

In this study, experiments to measure nitrogen-water two-phase relative permeabilities were conducted at a room temperature of around $20^{o}C$. The slip factors of nitrogen and steam flow through porous media were measured at different temperatures up to about $170^{o}C$.

Rock and Fluids. Berea sandstone was used in this study. The Berea core was fired at high temperature to remove the clay. The permeability and porosity of the rock were 1.28 darcy and 23.4%; the length and diameter were 43.2 cm and 5.08 cm respectively. The reason for the use of long core was to reduce the end effect. If the core sample is too short, the end effect may significantly influence the calculation of gas relative permeabilities.

Brine of 1.0 percent (wt) NaCl was used as the liquid phase and nitrogen the gas phase in the experiments of measuring nitrogen-water relative permeabilities; the brine specific gravity and viscosity were 1.01 and 1.0 cp at $20^{o}C$. Distilled water was injected to generate steam in the experiments measuring the steam slip factor.

Experimental Apparatus. The schematic of the apparatus used to measure nitrogen-water relative permeabilities by a steady-state method is shown in Figure 3.1. For the water phase, the system was closed. The decrease (or increase) of water volume in the core was equal to the increase (or decrease) of water volume in the container at the core outlet on Balance 1 (assuming that the water phase is incompressible). Balance 1 had an accuracy of 0.01 g and a capacity of 1600 g. Water saturations in the core were then calculated using Eq. 3.15 with the data from Balance 1. Another balance (Balance 2 in Figure 3.1) was used to weigh the coreholder directly to verify the results obtained by Balance 1. Flexible tubings for fluid injection at the inlet and for production at the outlet were used to connect to the core so that the decrease (or increase) of the coreholder

weight would be directly proportional to the decrease (or increase) of water saturations in the core. Therefore, the water saturations in the core could also be measured by Balance 2; this balance had an accuracy of 0.1 g and a capacity of 6000 g. We found that the water saturations measured by the two balances were closely equal to each other.
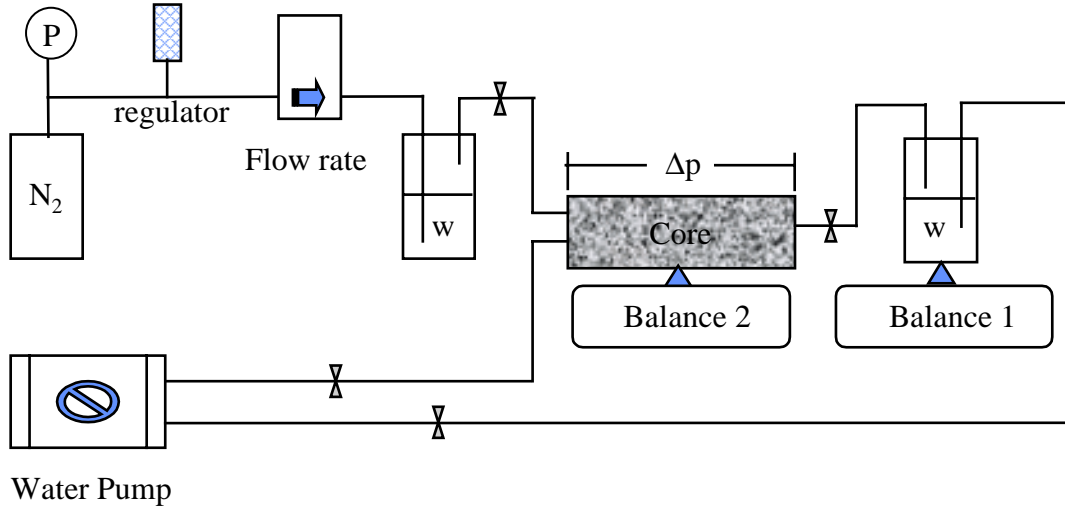
Figure 3.1: Schematic of gas-water relative permeability steady-state test.

Figure 3.2 shows the schematic of the apparatus developed to measure the slip factors of both the steam and nitrogen at high temperatures. The balance (the same as Balance 2 in Figure 3.1) in Figure 3.2 was used to monitor the water saturation in the core sample. The flow rates of steam at both inlet and outlet of the core can be calculated using the water injection or production rates, the steam temperature, and pressure measured during the experiments. The steam flow rates at the inlet and outlet were equal. The purpose in measuring at both ends was to monitor if there were problems such as leakage in the coreholder system. The coreholder and the method to assemble the core sample used in this study were similar to those of Satik and Horne (1998).
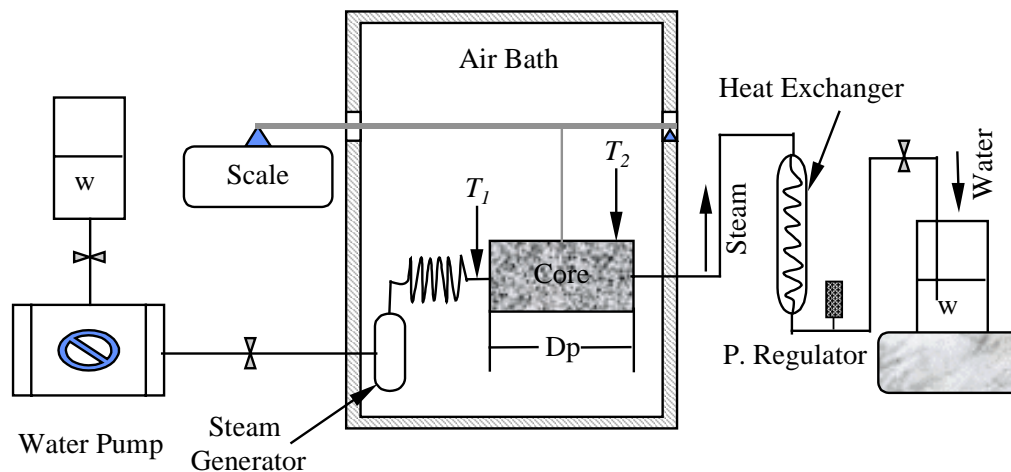
Figure 3.2: Schematic of gas (nitrogen and steam) slip factor test.

Procedure. The core sample was first dried by evacuation. The weight of the coreholder was monitored using a balance with an accuracy of 0.1 g. The core was assumed to be dry when its weight did not change in eight hours of evacuation at a vacuum of about 30 millitorr. Then the gas permeabilities were measured at different mean pressures using nitrogen. Following that, the core was completely saturated with 1% (wt) NaCl brine by evacuation and the absolute liquid permeability of the core was measured after several pore volumes of brine were injected. Next, steady-state relative permeability experiments were started and varying fractions of nitrogen and water were injected into the core. Measurements at each fraction resulted in a single data point on a relative permeability vs. water saturation curve. In this study, the experiment commenced from a water saturation of 100%. The water saturations were reduced by increasing the fraction of gas in the injected fluids, which formed a drainage relative permeability curve. The nitrogen relative permeabilities were measured at different mean pressures but at the same saturation. After the relative permeability experiments were completed, the core was dried again and the nitrogen slip factors were measured at temperatures ranging from 20 to 120°C. Following that, the core was evacuated for 24 hours at about 30 millitorr to get rid of the nitrogen in the core sample. The steam slip factors were then measured at temperatures ranging from 120 to 170°C.

3.5 RESULTS

Nitrogen-water relative permeabilities were measured at ambient conditions. It was found that some values of relative permeabilities of the gas phase were greater than one at certain low water saturations due to gas slippage. We also conducted experiments at high temperatures to measure the slip factors of both nitrogen and steam flow in porous media. The results are discussed in this section.

Nitrogen-Water Relative Permeability. Figure 3.3 shows the effect of mean pressure in the core on gas (nitrogen) relative permeabilities calculated without considering the gas slip effect in two-phase flow. Gas relative permeabilities were measured at different mean pressures ranging from 1.05 to 1.40 atm. The water saturations were less than 31.8%. The reason for this was the difficulty in keeping water phase immobile at water saturations above 31.8%. The effect of mean pressure on gas relative permeabilities was significant (see Figure 3.3). Most of the gas relative permeabilities measured at these pressures were greater than one. This was because the gas slip effect was not considered in calculating gas relative permeabilities while the absolute permeability (measured by water injection) was used as the specific permeability.

The relationship between the apparent gas permeabilities and the reciprocal of mean pressure at different water saturations ranging from 0 to 31.8% was shown in Figure 3.4. A linear correlation between the gas permeabilities and the reciprocal of mean pressure exists at all the tested water saturations.
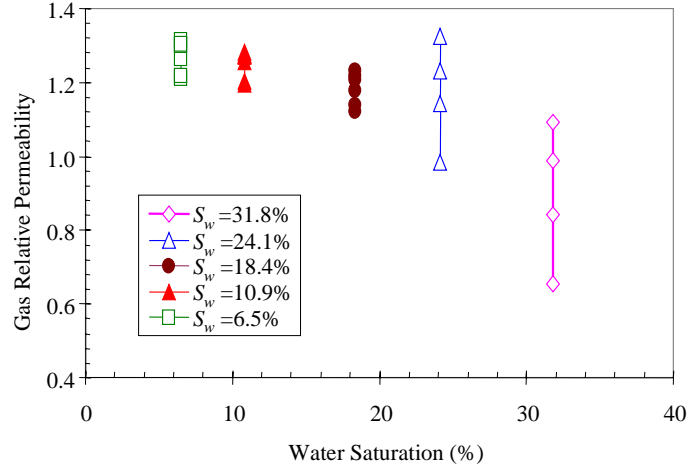
Figure 3.3: Effect of gas slippage on gas relative permeabilities in nitrogen-water systems.
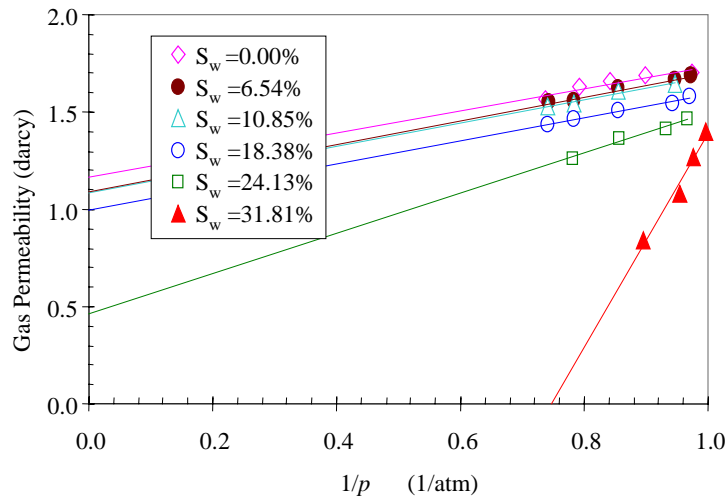
Figure 3.4: Gas slippage effect at different water saturations.

The intrinsic gas permeability at zero water saturation is calculated by a linear regression on the experimental data. The computed intrinsic gas (nitrogen) permeability, that is, the gas permeability corresponding to an infinite pressure, $k_{g\infty}$, is equal to 1.275 darcy and close to the absolute liquid permeability of 1.280 darcy measured using 1% (wt) NaCl brine. It can be also seen from Figure 3.4 that the water saturation has a significant effect on the intrinsic effective gas permeability. Note that the intrinsic effective gas permeability at the water saturation of 31.8% is negative if a linear relationship between the apparent gas permeability and the reciprocal of mean pressure is assumed. The reason for this may be due to mobility of the water at such a high water saturation. If water flows, the theory of gas slippage may need to be modified.

The gas (nitrogen) slip factors at different water saturations were calculated using the data shown in Figure 3.4 and the results are presented in Figure 3.5. The data point at the

water saturation of 31.8% was removed due to the unusual value of the intrinsic effective gas permeability. The gas slip factor increases with water saturation although it does not vary much at water saturations in the range 0 to 18.4%. All the previously mentioned authors (Rose, 1948; Fulton, 1951; Estes and Fulton, 1956) reported that the gas slip factor decreases with an increase of water saturation, which seems against the Klinkenberg theory.
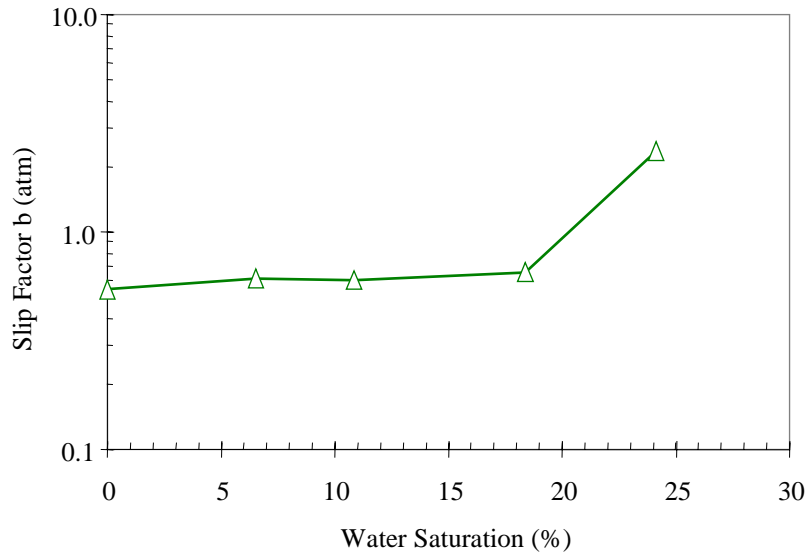
Figure 3.5: Effect of water saturation on Gas slip factor.

Figure 3.6 plots the computed gas slip factors vs. the corresponding intrinsic effective gas permeabilities at different water saturations. Interestingly, a linear relationship between the gas slip factor and the intrinsic effective gas permeability is observed on a log-log plot. The gas slip factor increases with the decrease of the intrinsic effective gas permeability This seems to be reasonable according to Eq. 3.5 even though Eq. 3.5 is based on experimental results for single-phase gas flow. Other authors (Rose, 1948; Estes and Fulton, 1956) found that the gas slip factor decreased with the intrinsic effective gas permeability, which is in contradiction to Eq. 3.5.

The drainage gas-water relative permeabilities over the whole range of water saturation are shown in Figure 3.7. The open triangles represent the drainage gas relative permeabilities at a mean pressure of about 1.4 atm. The intrinsic gas relative permeabilities are calculated using Eq. 3.10 and plotted in Figure 3.7 as solid circles. The corrected intrinsic gas relative permeabilities of gas phase are always less than one. The gas relative permeability function at any mean pressure, $k_{rg}(S_w, p_m)$, can be computed using Eq. 3.11 once the intrinsic gas relative permeabilities and the gas slip factors at different water saturations are available.
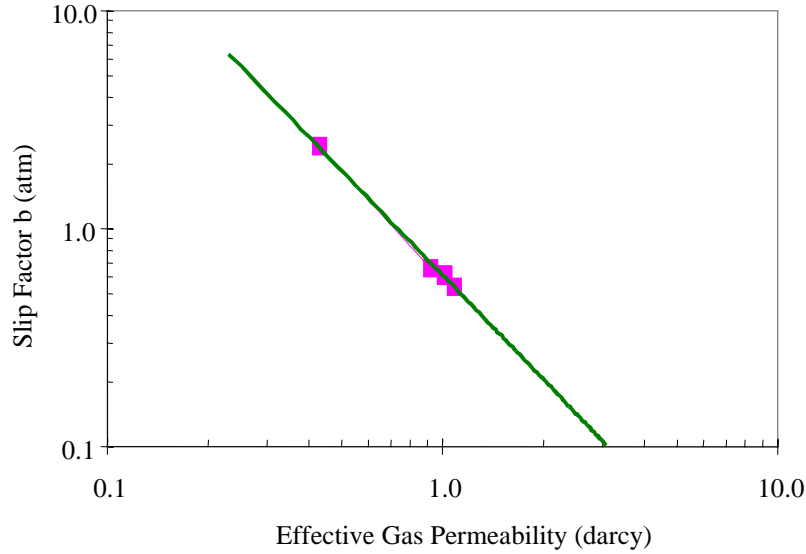
Figure 3.6: Relationship between gas slip factor and intrinsic effective gas permeabilities.
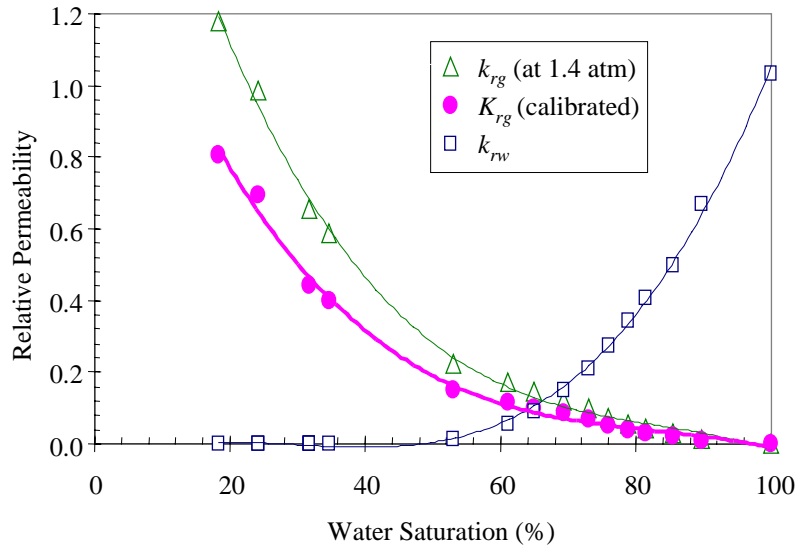
Figure 3.7: Gas slippage effect on nitrogen-water relative permeabilities.

If reservoir pressure is close to or above the pressure at which the gas slip effect can be neglected, the gas relative permeabilities at reservoir conditions can be represented by the intrinsic gas relative permeabilities calculated using Eq. 3.10. Otherwise, the gas relative permeability function in the reservoir should be computed using Eq. 3.11. For example, Fort (1992) reported that the reservoir pressure near the wellbore in the West Panhandle Gas Field had dropped to about 1 atm due to the area-wide vacuum operations. In such a case, gas slip effect had to be included in reservoir engineering calculations. Another example is the application of thermal vacuum wells in the remediation of deep soil contamination (Stegemeier, 1992; Vinegar, 1997). In this case, the reservoir pressure was very low and the temperature was very high (258°C). The gas slip effect was not negligible under such reservoir conditions. In geothermal reservoirs, reservoir pressure

22

may not be significantly above the higher pressure limits where gas slippage can be neglected. Therefore, the gas slip effect may not be neglected due to the low permeabilities and high temperatures. From these examples, it is seen that gas slip effect may be not only an experimental consideration but also a matter of reservoir engineering in both single-phase and two-phase flow.

Effect of Temperature. Figure 3.8 shows the effect of temperature on the apparent nitrogen permeabilities measured using the apparatus shown in Figure 3.2. The temperature ranged from room temperature to about 120^oC. The apparent nitrogen permeabilities at specific pressures increase with temperature. The intrinsic permeabilities (at infinite mean pressure) at different temperatures are equal, around 1.20 darcy. This intrinsic permeability is close to but less than the absolute permeability (1.28 darcy) measured by water flow. Figure 3.8 demonstrates that the nitrogen slip factor increases with temperature. These results are consistent with those reported by Wel *et al.* (1982); their measurements were made at a lower range of temperature from 0 to 63^oC.
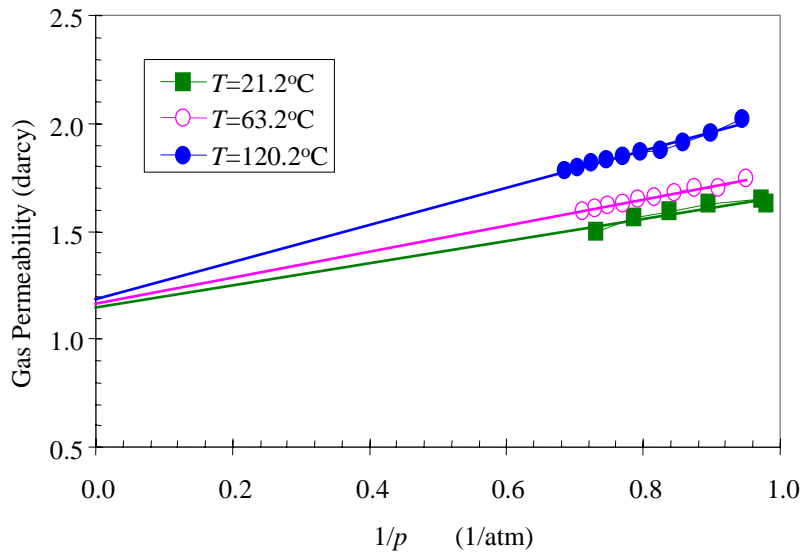
Figure 3.8: Gas (nitrogen) slip effect at different temperatures.

The apparent steam permeabilities in the Berea sandstone at three different temperatures (120.1, 150.8, and 170.2^oC) were measured using the apparatus shown in Figure 3.2. The results are demonstrated in Figure 3.9. The apparent steam permeabilities at specific pressures also increase with temperature. The intrinsic permeabilities of steam at the three different temperatures are almost equal to each other and close to the absolute permeability measured by brine injection. The steam slip factor increases with temperature, too.
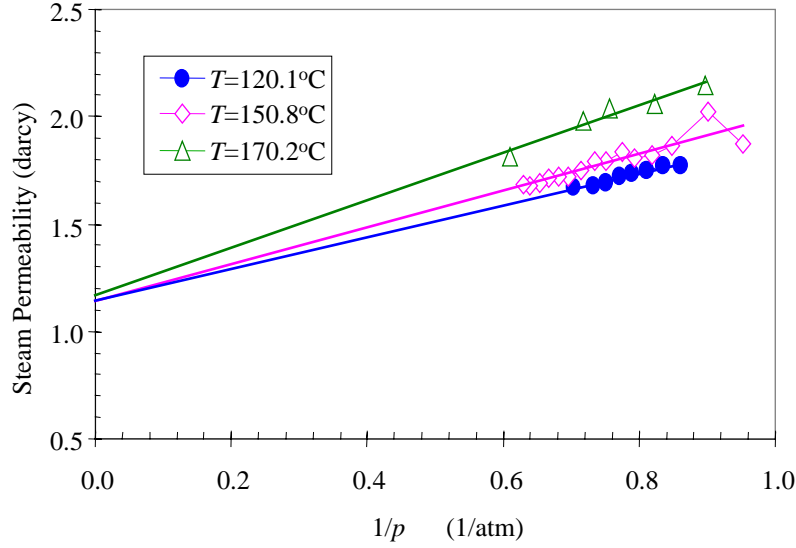
Figure 3.9: Gas (steam) slip effect at different temperatures.

Figure 3.10 shows the comparison of the relationship between the gas permeability and the reciprocal of mean pressure of nitrogen to steam at a temperature of about 120°C. The permeabilities and the slip factor of nitrogen are greater than those of steam at specific pressures. Amyx *et al*. (1960) stated that the data obtained with lower molecular weight gas yield a straight line with greater slope, indicative of a greater slippage effect. The molecular weight of nitrogen is greater than steam but the nitrogen slip factor is greater than that of steam, as shown in Figure 3.10. Actually, this is reasonable, as analyzed in the following. The gas slip factor in a circular capillary tube can be expressed as follows (Rose, 1948):

$$b = \frac{32}{3\pi} \sqrt{2\pi} \frac{\mu c}{r} \sqrt{\frac{RT}{M}} \qquad (3.17)$$

where μ is the gas viscosity, R is the gas constant, T is the absolute temperature, and M the molecular weight of gas. For nitrogen and steam, the following equation applies:

$$\frac{b_{N_2}}{b_S} = \frac{\mu_{N_2}}{\mu_S} \sqrt{\frac{M_S}{M_{N_2}}} \qquad (3.18)$$

where b_{N_2}, μ_{N_2}, and M_{N_2} are the slip factor, viscosity, and molecular weight of nitrogen; b_S, μ_S, and M_S are the slip factor, viscosity, and molecular weight of steam. The viscosities of nitrogen and steam at a temperature of 120°C are 0.021 cp and 0.013 cp respectively. The ratio of nitrogen slip factor to the steam calculated using Eq. 3.18 would be about 1.295. This shows that the nitrogen slip factor should be greater than that of steam at the same temperature, as shown in Figure 3.10. The ratio of nitrogen slip factor to the steam calculated using the data presented in Figure 3.10 is about 1.124, close to the theoretical value in a circular capillary tube.

24
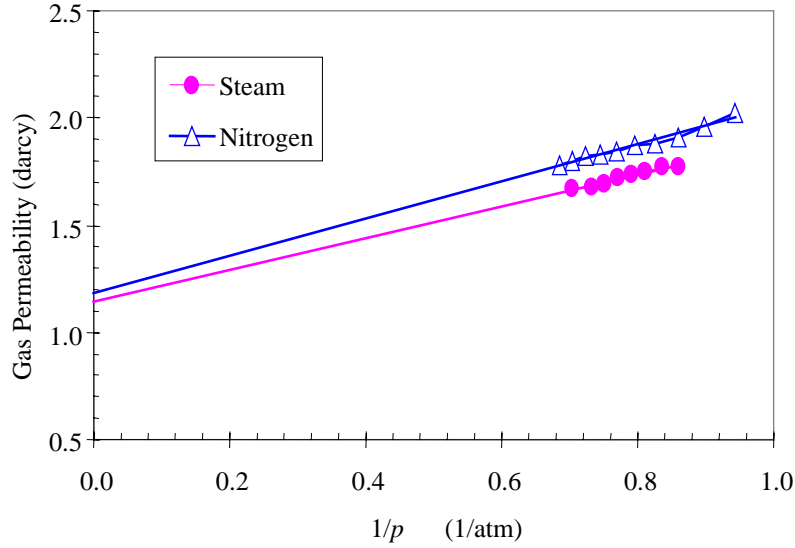
Figure 3.10: Comparison of nitrogen slip effect to steam at a temperature of 120°C.

The effects of temperature on both nitrogen and steam slip factors are plotted in Figure 3.11. As we discussed previously, both nitrogen and steam slip factors increase with temperature. Nitrogen slip factor is greater than that of steam. Therefore, it may not be appropriate to substitute steam slip factor using that of nitrogen or other gases.
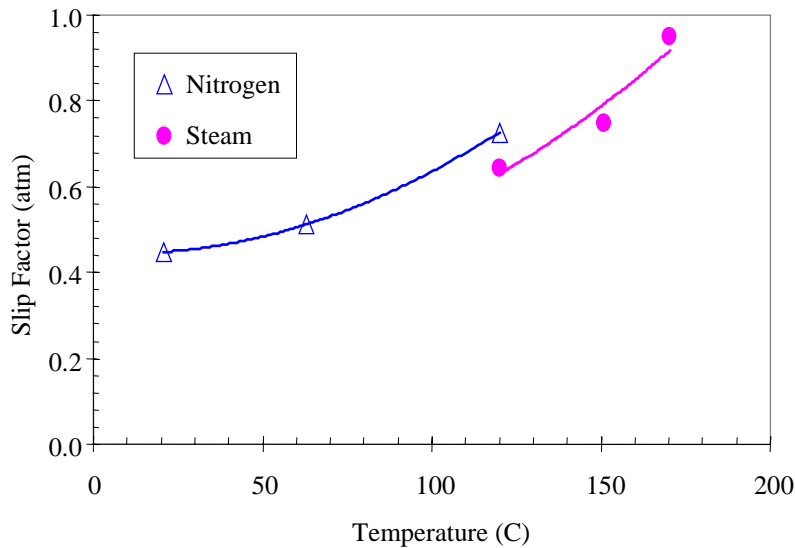
Figure 3.11: Effect of temperature on nitrogen and steam slip factor.

Correction of Steam Phase Relative Permeability. Steam-water relative permeabilities are usually measured at high temperatures above 100°C. Gas slip effect in steam-water flow may also be significant due to the high temperature. Satik and Horne (1998) found that steam relative permeabilities at some water saturations appeared to be greater than unity. Mahiya (1999) also observed a similar phenomenon. This can be attributed to the gas slip effect in steam-water flow. The uncorrected steam-water relative permeabilities

measured by Mahiya (1999) are shown in Figure 3.12 as the open triangles. We measured the steam slip factor using a similar Berea sandstone core which had almost the same permeability as the core Mahiya (1999) used. The value of the steam slip factor at a temperature of 120°C, the average temperature at which steam-water relative permeabilities were measured, was about 0.647 atm. The steam relative permeabilities measured at the pressure close to the atmospheric were corrected using this value of the steam slip factor and the corresponding mean pressure; the corrected intrinsic steam relative permeabilities are plotted in Figure 3.12 as the solid circles. The steam slip factor was assumed to be constant at all water saturations due to the lack of data. It can be seen from Figure 3.12 that all the corrected steam relative permeabilities are less than one. The gas (steam) slip effect in steam-water two-phase flow is significant.
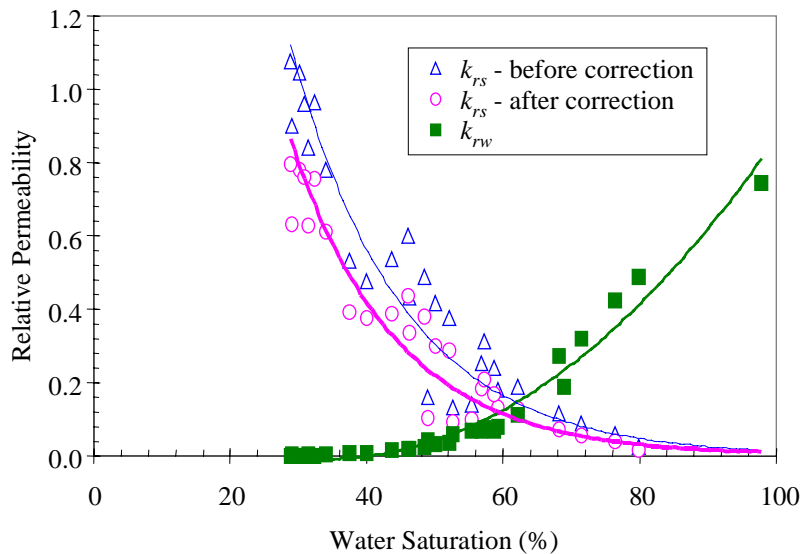
Figure 3.12: Calibration of steam relative permeabilities in steam-water flow.

3.6 DISCUSSION

As a matter of experimental practicality, steam-water or gas-water relative permeabilities are usually measured at a low mean pressure. When the gas-liquid relative permeabilities are reported to the reservoir engineers, the corresponding experimental mean pressures may not be included within the report. It is known from the analysis reported here that gas relative permeabilities may change with the mean pressure. The reservoir pressure is generally much different from the experimental pressure. So, if reservoir engineers apply the experimental data of relative permeabilities in reservoir calculations, significant error may occur. The solution to this problem is clear. The intrinsic gas relative permeabilities independent of test mean pressure should be computed and reported to reservoir engineers together with the corresponding steam slip factors and the test pressures. Therefore, reservoir engineers can use Eq. 3.11 to calculate the gas relative permeabilities at whatever pressures are required.

As discussed previously, gas slip effect is not only an experimental consideration but also a matter of reservoir engineering if the reservoir pressure is not well above the higher pressure limits where gas slippage can be neglected. Examples are the gas reservoirs under vacuum operation and reservoirs with extremely low permeabilities. Pressure and water saturation change very much in a reservoir. Therefore, fluid flow calculations for these reservoirs should take account of the gas slip effect as a function of pressure and water saturation. Ertekin *et al* (1983) developed such a fluid flow model in which a dynamic slip factor (pressure and saturation dependent) was included. This model would be helpful to modifying numerical simulators in gas reservoirs under vacuum operation and reservoirs with extremely low permeabilities.

Unfortunately, the experimental data of gas slip effect in two-phase flow are few and inconsistent. There are many issues to be solved in this field. For example, the relationship between the gas permeability and the reciprocal of mean pressure is not yet clear when the water phase is mobile. On the other hand, little attention has been paid to the effect of capillary pressure on the calculation of gas relative permeabilities, which may be significant when the core studied is short and very low permeable.

3.7 CONCLUSIONS

Based on the present work, the following conclusions may be drawn:

1. Gas slippage affects gas (both nitrogen and steam) relative permeability significantly; neglecting the gas slip effect in gas-liquid two-phase flow will overestimate gas relative permeability values.
2. The gas slip factor increases with the water saturation but is almost constant at water saturations below about 18%.
3. A linear correlation between the gas slip factor and the effective intrinsic gas permeability was observed on a log-log plot.
4. Both the nitrogen and steam slip factors increase with temperature. The steam slip factor is less than that of nitrogen at the same temperature.
5. It may be necessary to calculate the intrinsic gas relative permeabilities independent of test pressures with the gas slip effect in two-phase flow considered.
6. Gas slip effect in both single- and two-phase flow is not only an experimental consideration but may also be of consequence in reservoir engineering calculations in some cases.

3.8 FUTURE WORK

The next step is to measure the gas slip factor when the water phase is mobile in the whole range of water saturation.

4. FRACTURED ROCK RELATIVE PERMEABILITY

This project is being conducted by Research Assistant Mark D. Habana, Research Associate Kewen Li and Prof. Roland N. Horne. The objective is to measure relative permeability relations for steam and water flow in a fractured geothermal rock. This work is an extension of current studies of steam-water flows which have so far considered only artificially uniform porous rocks. As a first step, nitrogen and helium flow was studied in a fractured Geysers core.

4.1 BACKGROUND

Various works on flow through fractures showed different kinds of relative permeability behavior. Experimental studies by Persoff and Pruess (1995) resulted in curves that could not be classified either as Corey type or as linear (X-curve) type. Fourar et al. (1993) suggested that multiphase interaction in a fracture is a function of flow velocity and therefore relative permeability is not the most appropriate way to describe multiphase flow in fractures.

Past experiments have used synthetic fabricated fractures and/or gas-water or oil-water as fluids. This experimental study will use a real fractured core from The Geysers geothermal field to study steam-water relative permeability.

Nitrogen and helium permeability experiments were conducted on the core to determine the effects of the rock fractures and to investigate the constraints and practicalities of conducting multiphase flow experiments in real geothermal rocks. The core contains several fractures as determined from an X-ray computer tomography image.

4.2 EXPERIMENTAL METHODOLOGY

The rock permeability was measured using nitrogen and helium gas at room temperature. The apparatus used is shown in Figure 4.1. Since gas permeability is a function of pressure, as described by Equation 4.1, the flow measurements were conducted at a series of different mean pressures.

$$k_{gas} = k_{abs}(1 - \frac{b}{p_{ave}}) \tag{4.1}$$

The core sample was obtained from a depth of 1409.3m at The Geysers geothermal field. The core is 6.91 cm in length and 4.70 cm in diameter.

At different confining pressures nitrogen was flowed into the core. Confining pressure from 500 to 850 psig was applied by injecting nitrogen around the heat shrink tubing inside the core holder. To apply a confining pressure of 1150 psig water was used in place of nitrogen.
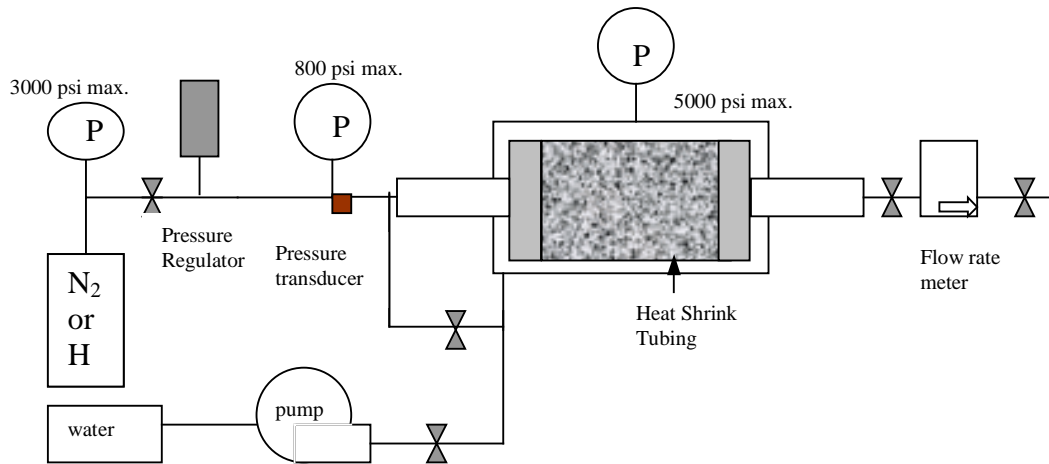
Figure 4.1: Apparatus for flow measurement in geothermal rock.

A pressure gauge and a pressure transducer connected to a digital display measured pressure at the inlet. The pressure at the outlet was taken to be 1 atm. The flow rate at the outlet was measured using a Matheson flow rate meter and controller (Model 8272-MF2000). The flow rate transducer calibration equation used was that determined by Kewen Li when he used the device in his experiments on slip factors (Oct-Dec 1999 Quarterly Report).

4.3 PARTIAL RESULTS AND DISCUSSION

The initial results are shown in Figure 4.2. The intersection of the extrapolated lines with the vertical axis in the plot of permeability (k) versus the reciprocal of the mean pressure ($1/p_{ave}$) is the taken to be the absolute permeability of the rock. The values of permeability range between 1 and 2 md.

It was observed that for the nitrogen experiments the permeability values decrease with increasing confining pressure. This can be attributed to the increase in net stress on the rock fractures as the confining pressure is increased. The increased net stress reduces the fracture aperture and, consequently, reduces the permeability.

For the helium experiment at a confining pressure of 850 psig the permeability obtained is higher than the values from the nitrogen experiments. Also, the slope for the helium experiment is lower than that for nitrogen at the same confining pressure. This is not as expected. The slope for helium should be much steeper than that for nitrogen considering the difference in viscosities and molecular weights of the two fluids. This disparity can be attributed to the flow transducer calibration equation used, which was obtained using nitrogen and therefore was not applicable to helium flow measurements. A new calibration is underway for helium flow.
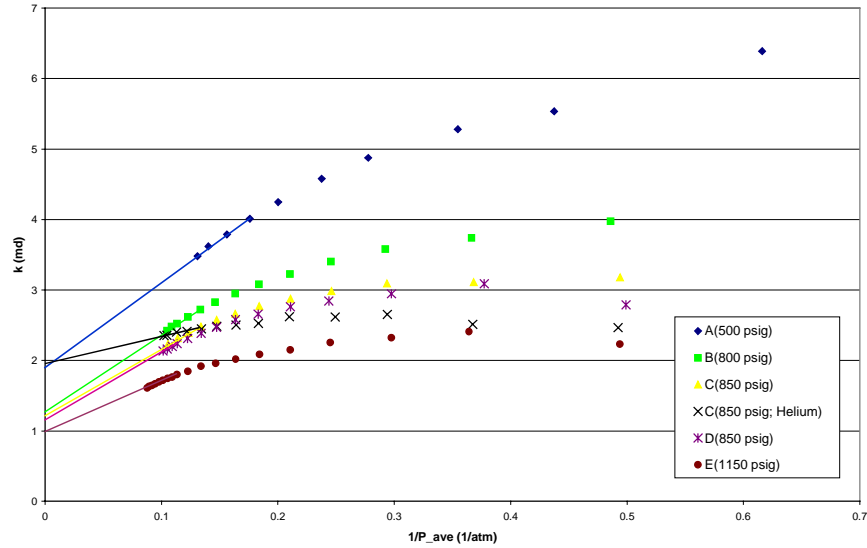
Figure 4.2: Results of nitrogen and helium permeability as a function of pressure.

Table 4.1: Absolute permeability results from preliminary nitrogen and helium experiments.

Fluid	Confining Pressure	Permeability
Nitrogen	500 psig	1.90 md
Nitrogen	800 psig	1.30 md
Nitrogen	850 psig	1.20 md
Helium	850 psig	1.95 md
Nitrogen	850 psig	1.15 md
Nitrogen	1150 psig	1.00 md

4.4 CONTINUING AND FUTURE WORK

TOUGH2 modeling will be undertaken prior to flowing water through the rock. After this, TOUGH2 models will also be made for steam-water flows in preparation for the steam-water relative permeability experiments.

The steam-water relative permeability experiment will be an unsteady-state displacement process. To make the experiment easier and faster an electrical resistivity tomography method is being developed to measure the saturations in the core – this approach should be more suitable than X-ray CT methods because of the likelihood of long duration of the experiments..

30

5. THE MEASUREMENT OF STEAM-WATER AND AIR-WATER CAPILLARY PRESSURE

This research project is being conducted by Research Assistant Chih-Ying Chen, Research Associate Kewen Li, and Professor Roland Horne. The aim is to measure steam-water and air-water capillary pressures, and attempt to distinguish the difference between them or confirm the difference is negligible. In the first stage, a simple experiment was conducted measuring capillary rise in narrow tubes. Preliminary data was acquired and will be used for future research reference.

5.1 BACKGROUND

Capillary pressure, an important but hard-to-measure physical property, plays a dominant role in reservoir performance and production forecasting. In the geothermal engineering field, the knowledge of the steam-water capillary pressure is limited because of difficulties in the measurement. Most of the difficulties come from the special phase relationship between the steam (water vapor) and the water. There is mass transfer between the steam and the water phase which makes conventional methods invalid or inaccurate. Horne et al. (1995) summarized the adsorption mechanism in geothermal reservoirs and described how adsorption curves could be used to infer capillary pressures. Sta. Maria and Pingol (1996), and Persoff and Hulen (1996) inferred values of steam-water capillary pressure from the adsorption data of Horne et al. (1995), and found steam-water capillary pressures ranging from 0 to 586 MPa (at 120ºC) and 0 to 190 MPa (at 28.5ºC) respectively. The difference between these two results is large. Li and Horne (2000) developed a mathematical model to calculate steam-water capillary pressure of geothermal rocks using the steady-state steam-water flow experiment, and the results obtained were consistent with those measured by Persoff and Hulen (1996).

A capillary rise experiment is a straightforward way to measure the capillary pressure. The schematic of capillary rise is shown in Figure 5.1. The capillary pressure can be obtained by using following equation:

$$P_c = \Delta\rho g h \tag{5.1}$$

where, $\Delta\rho = \rho_w - \rho_g$ denotes the difference in density between water phase and gas phase; g is the gravity constant and h is the height of the capillary rise to the meniscus above a flat liquid surface. The density of air is 0.0014 g/cm^3 (at 20ºC), whereas the density of steam is about 0.00075 g/cm^3 (at 20ºC). The density difference between air-water and steam-water systems seems very small, so we should consider whether the difference between air-water and steam-water capillary pressure is significant or not. If the density difference is not significant, the air-water capillary pressure could be used as a substitute for the steam-water capillary pressure. However, if the difference is significant, it is necessary to develop a more accurate and efficient method to measure the steam-water capillary pressure.
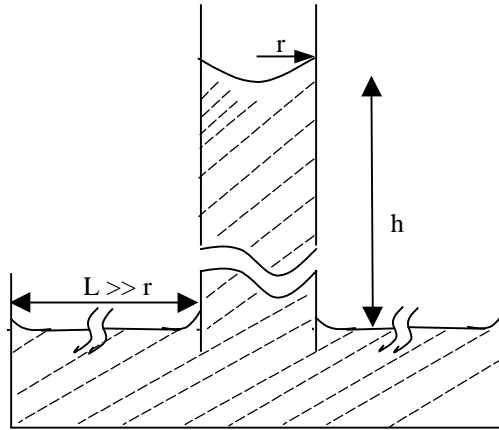
Figure 5.1: Capillary rise phenomenon (not to scale).

5.2 EXPERIMENT APPARATUS

In the first stage, a capillary rise experiment was implemented to test whether any difference between air-water and steam-water capillary pressures can be distinguished. The apparatus of the capillary rise experiment is shown in Figure 5.2. The concept of this experiment is based on the capillary rise phenomenon (see Figure 5.1). The five capillary tubes used in this experiment were Fisher 5 microliter borosilicate glass pipettes (Cat. No. 21-764-2B, TC $\pm$ 0.5% accuracy) with average diameter 0.027cm, and length 12.7cm. Two plastic rulers with accuracy 1mm were used to measure the height of the capillary rise and water table. All of the tubes and rulers were adjusted to the same readings at the same height and were fixed to an aluminum bar which bridged the beaker horizontally. A vacuum pump (Welch Technology, Inc., Model 8915) was used to remove the air inside the chamber when measuring the steam-water capillary pressure (see Figure 5.2). A pressure transducer was installed to monitor the vacuum state and measure the pressure in the chamber.

The air-water capillary pressure was measured first in the open environment (room temperature) by adding distilled water into the beaker assembly (beaker, aluminum bar attached with capillary tubes and rulers, and thermometer). The air-water capillary pressures were measured by reading the height of the menisci on the rulers. After that, the beaker was dried and the water trapped in the tubes was flushed out by injecting air- for 1 minute. Then, the beaker set was put into the chamber, and the vacuum pump was started to evacuate the chamber to around 50 minitorr for 1 hour. After vacuuming, distilled and deaerated water was introduced into the beaker. At this moment, some water in the beaker evaporated into the space of the chamber. This phenomenon could be detected from a slight rise of the near-vacuum pressure. After the beaker was filled with sufficient water to immerse the tubes, the water valve was closed (see Figure 5.1). The steam-water capillary pressure was recorded starting at this time until several days later.
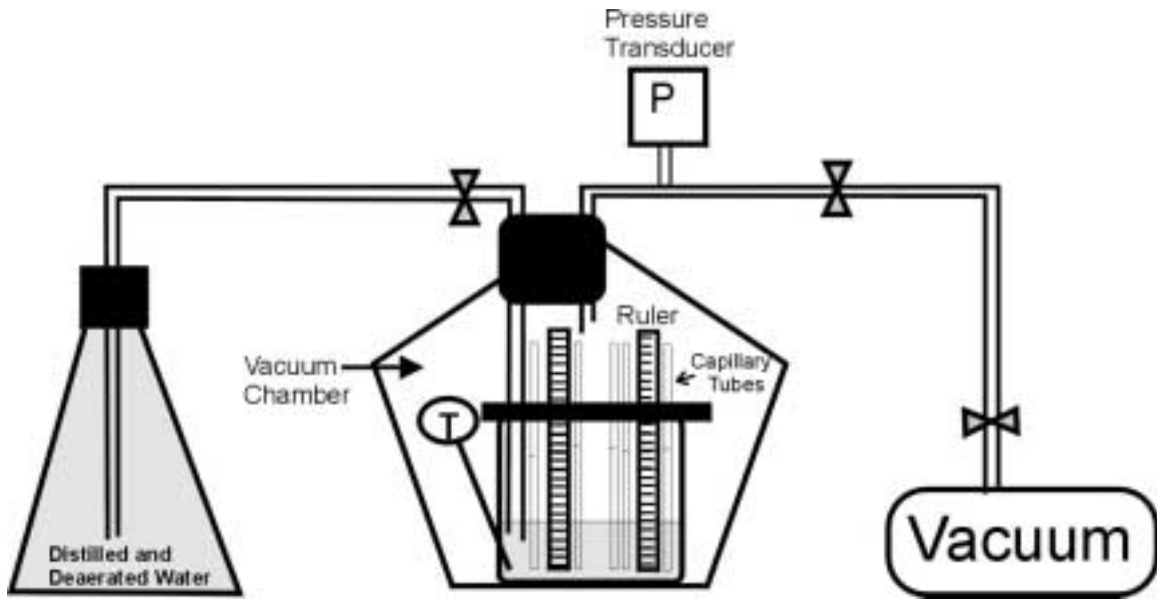
Figure 5.2: Schematic of apparatus of measuring steam-water and air-water capillary pressure.

5.3 PARTIAL RESULTS AND DISCUSSION

The measured air-water and steam-water capillary pressures are shown in Table 5.1. The average air-water capillary pressure measured in this experiment was 31.6mm, and the average steam-water capillary pressure was 30.76mm. Only a slight difference between air-water and steam-water capillary pressure was found in this experiment. As can be seen in Table 5.1, the air-water capillary pressure measured in each tube is higher than the steam-water capillary pressure measured in the same tube. Air-water capillary pressure is higher on average than steam water capillary pressure by 0.84 mm. Tube 2, tube 4, and tube 5 had the largest difference (1.0mm), whereas tube 1 had only a small difference (0.5mm). However it is not clear from these measurements whether these differences were attributable to differences between the air-water and steam-water capillary pressure. This is because some problems were found during this experiment when measuring the capillary pressure. The problems are attributed to: (a) the capillary balance time; (b) the hysteresis between imbibition and drainage; (c) the quality of the tubes.

A series of capillary tests was conducted in order to reduce experimental errors and uncertainty. Some factors that may affect the capillary measurement should be addressed. Figure 5.3 shows the steam-water capillary rise vs. time in two of our testing tubes, A and B. In tube B, it took less than 4 hours to reach equilibrium. However, the height in tube A increased continuously, even after 1 week of measurements. This abnormal phenomenon occurred in some of the tubes. The reason is still under investigation. The hysteresis of imbibition and drainage processes is another important factor that governs the capillary rise. During our steam-water capillary pressure measurement, a slight descent of the water table owing to the water inside the chamber evaporation was measured. However, a corresponding descent of capillary rise could not be measured. This phenomenon could

be explained by the hysteresis between the imbibition and drainage processes. The hysteresis is related to the advancing and receding contact angles. Theoretically, the capillary pressure in the drainage process will be larger than in the imbibition process. In our case, the lowering of the water table is related to the drainage process. The hysteresis could be a source of experimental error, since according to Table 5.1, the difference between air-water and steam-water capillary pressure is near the ruler's minimum tick (1mm) and our visual measurement limit (0.5mm). Furthermore, the capillary pressure in different tubes ranged from 27 mm to 34 mm. This may be because the tubes were not uniform or each part of one tube has slight radius change. A skeptical attitude is still held at this preliminary stage.

Table 5.1: Measured air-water and steam-water capillary pressures

	T (°C)	Pressure (psi)	Water Table (mm)	Tube 1 reading	Tube 1 Capillary Pressure	Tube 2 reading	Tube 2 Capillary Pressure	Tube 3 reading	Tube 3 Capillary Pressure	Tube 4 reading	Tube 4 Capillary Pressure	Tube 5 reading	Tube 5 Capillary Pressure
Air-water Experiment	22	14.7	31.5	61	29.5	63.5	32	65	33.5	66.5	35	59.5	28
Steam-water Experiment	22	~0	32	61	29	63	31	64.8	32.8	66	34	59	27
Capillary Pressure Difference					0.5		1		0.7		1		1

* pressure unit is mm H2O
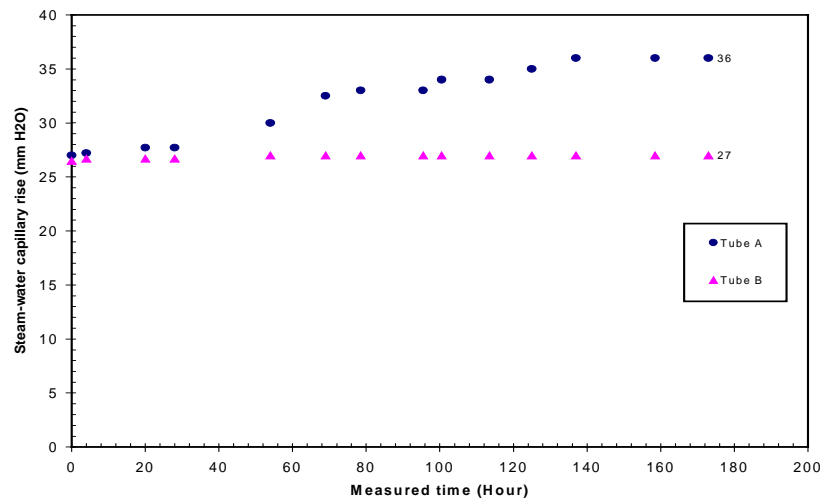
Figure 5.3: Steam-water capillary rise vs. time under 2 weeks measurement in tubes A and B.

5.4 FUTURE WORK

The result of this preliminary experiment shows that air-water capillary pressure may be higher than steam-water capillary pressure by a small difference, but no definitive

conclusion is possible at this stage. Further research will focus on the theoretical surface chemistry and thermodynamics governing air-water and steam-water capillary interfaces, and the next experiment will be conducted on a system with a porous rock sample. This more practical experiment has been designed to use a ceramic core sample of well-prescribed properties. A schematic of the new experiment is shown in Figure. 5.4. This apparatus will be used to measure the air-water and steam-water capillary pressure of the ceramic core sample at different water saturations.
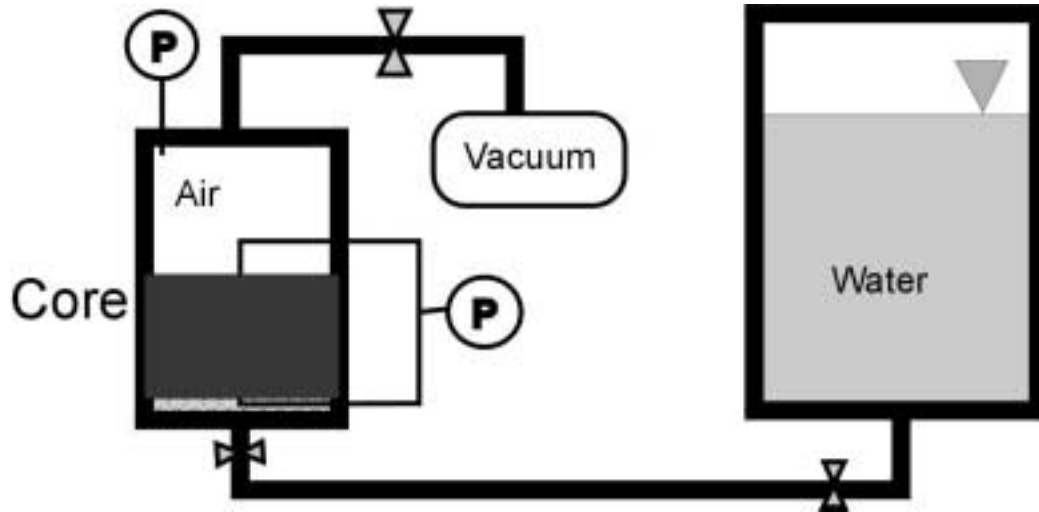
Figure 5-4: Schematic of the air-water and steam-water capillary pressure measurement in a ceramic core sample.

6. EXPERIMENTAL INVESTIGATION OF STEAM AND WATER RELATIVE PERMEABILITY ON SMOOTH WALLED FRACTURE

This project is being conducted by Research Assistant Gracel P. Diomampo, Research Associate Kewen Li and Prof. Roland Horne. The goal is to gain better understanding of steam-water flow through fractured media and determine the behavior of relative permeability in fractures.

6.1 BACKGROUND

Geothermal reservoirs are complex systems of porous and fractured rocks. Complete understanding of geothermal fluid flow requires knowledge of flow in both types of rocks. Many studies have been done to investigate steam and water flow through porous rocks. This is not the case for multiphase flow in fractures. Only a few published data are available most of which have been done for air-water system or for water-oil systems. An early study was Romm's (1966) experiment with kerosene and water through an artificial parallel-plate fracture lined with strips of polyethylene or waxed paper. Romm found a linear relationship between permeability and saturation, $S_w = k_{rw}$, $S_{nw} = k_{rnw}$ such that $k_{rw} + k_{rnw} = 1$. Pan et al. (1996) performed a similar experiment with an oil-water system but arrived at conflicting results. Significant phase interference was observed such that $k_{rw} + k_{rnw} < 1$. Both studies, however, conclude that residual saturations are zero such that a discontinuous phase can flow as discrete units along with the other phase.

In an attempt to develop a relationship between fracture relative permeability and void space geometry, Pruess and Tsang (1990) conducted numerical simulation for flow through rough-walled fractures. Their study showed the sum of the relative permeabilities to be less than 1, residual saturation of the nonwetting phase to be large and phase interference to be greatly dependent on the presence or absence of spatial correlation of aperture in the direction of flow. Persoff et al. (1991) conducted experiments on gas and water flow through rough-walled fractures using transparent casts of naturally fractured rocks. The experiment showed strong phase interference similar to flow in porous media. Data of Persoff (1991) and Persoff and Pruess (1995) for flow through rough-walled fractures were compared in Horne et al. (2000), as shown in Figure 6.1.

As a consequence of the disagreement between these earlier studies, the mechanism of flow and the characteristic behavior of relative permeability in fractures are still undetermined. Issues such as whether a discontinuous phase can travel as discrete units carried along by another phase or will be trapped as residual saturation as in a porous medium are unresolved. The question of phase interference i.e. whether the relative permeability curve against saturation is an X-curve, Corey curve or some other function is still unanswered. The main objective of this study is to contribute to the resolution of these issues. Experiments on flow through smooth-walled fractures will be done first for air-water flow with the aim of establishing a reliable methodology for flow characterization and permeability calculation. Then these experiments will be done with a steam-water system; and with rough-walled fractures.
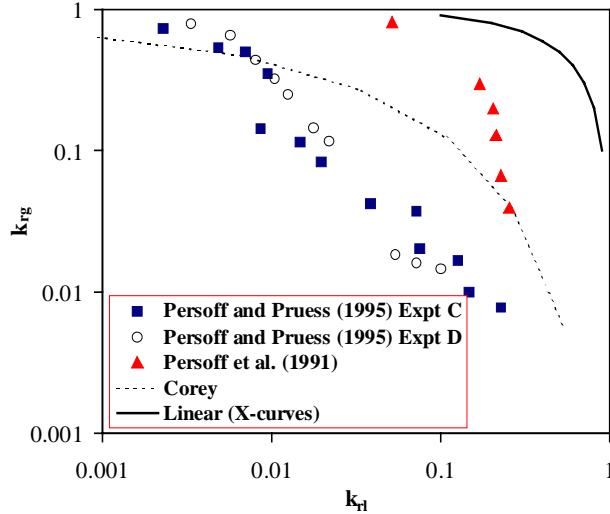
Figure 6.1 Measurements of air-water relative permeabilities in rough-walled fractures (graph from Horne et al. (2000))

6.2 EXPERIMENTAL APPARATUS AND MEASUREMENT TECHNIQUES

The apparatus consists of a 183 cm. by 31 cm of horizontal glass plate on top of an aluminum plate. The aperture is set by 0.2-mm thick shims inserted in between the glass and aluminum plates. The shims were placed along the boundaries and in three columns along the flow area. It should be noted that the shims placed as columns along the plate do not divide the plate into separate flow sections. This was determined upon observing cross flow along the shims.

The sides of the plates were sealed together with a silicone adhesive. It was observed that even with the adhesive, the inlet pressure head had to be kept below 15 cm to avoid leakage. A vacuum of 0-5 psig was applied at the two-phase outlet. This created greater pressure drop without increasing the inlet head. Pulling a vacuum allows more flexibility with flow rate and helps prevent leakage.

Horizontal slits in the ends of the metal plate served as entry and exit points for the fluids. There were two available canals for input of gas and liquid. The options to inject nitrogen and water as separate streams or as mixed fluid in a single stream were tried. It was found that mixing the gas and water prior to input caused no significant improvement in fluid distribution. Thus, the gas and water streams were injected separately for simplicity, ease of flow rate control and inlet pressure reading.

Gas flow was controlled through a flow regulator. A meter pump controlled the rate of liquid injection. Dye was dissolved in the injection reservoir for better phase identification. Figure 6.2 is a schematic diagram of this configuration.
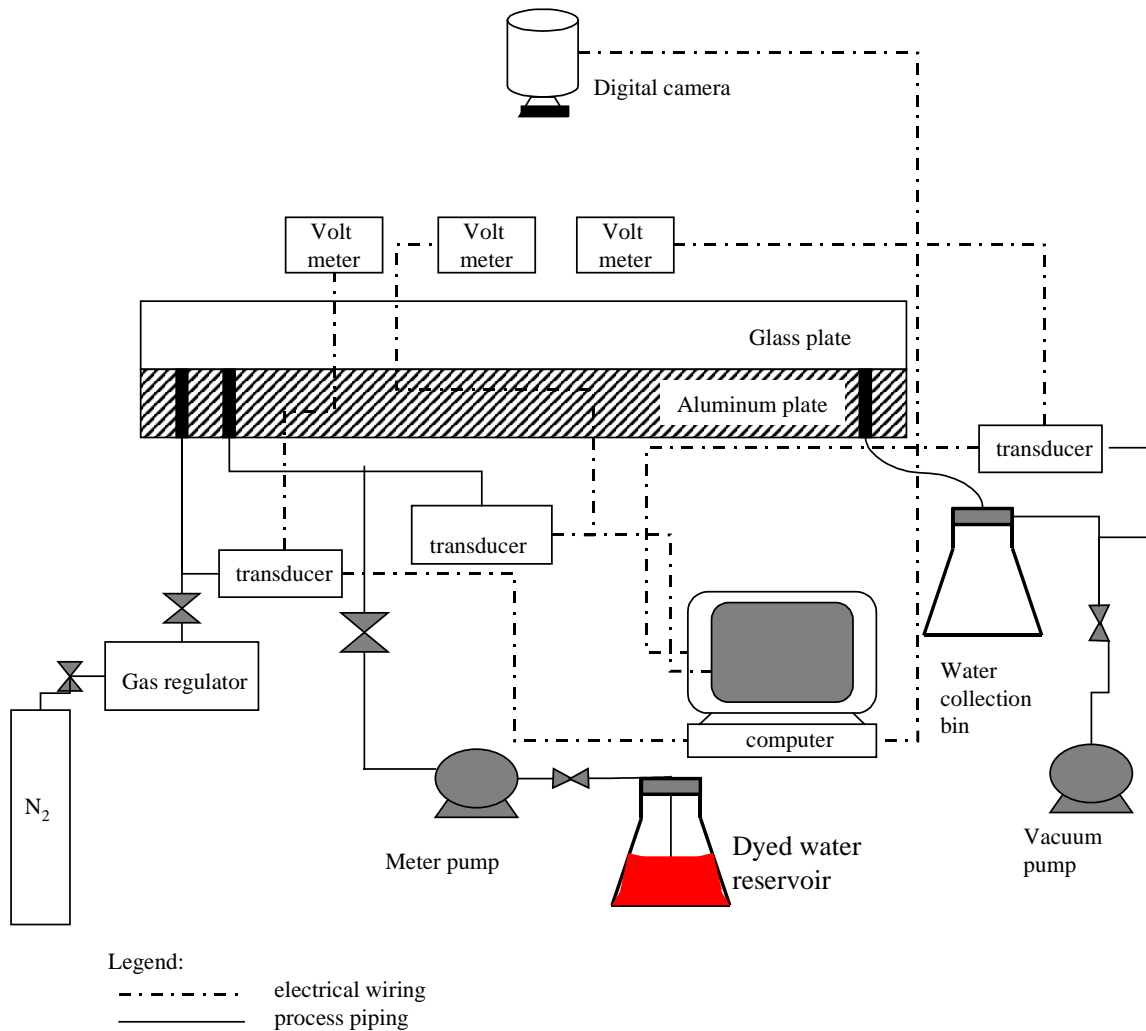
Figure 6.2: Experimental apparatus for air and water flow through smooth walled fractures

Water rate was read from the pump meter and gas rate from the regulator. Low range transducers measured the gas, liquid inlet pressure and the two-phase outlet pressure separately. These transducers were attached to a Labview program designed to record data at user-specified time interval. Attached to each transducer was a voltmeter. The reading of the voltmeters is recorded by the video camera together with a visual image of the two-phase flow. This is to gather the instantaneous pressure and saturation data simultaneously.
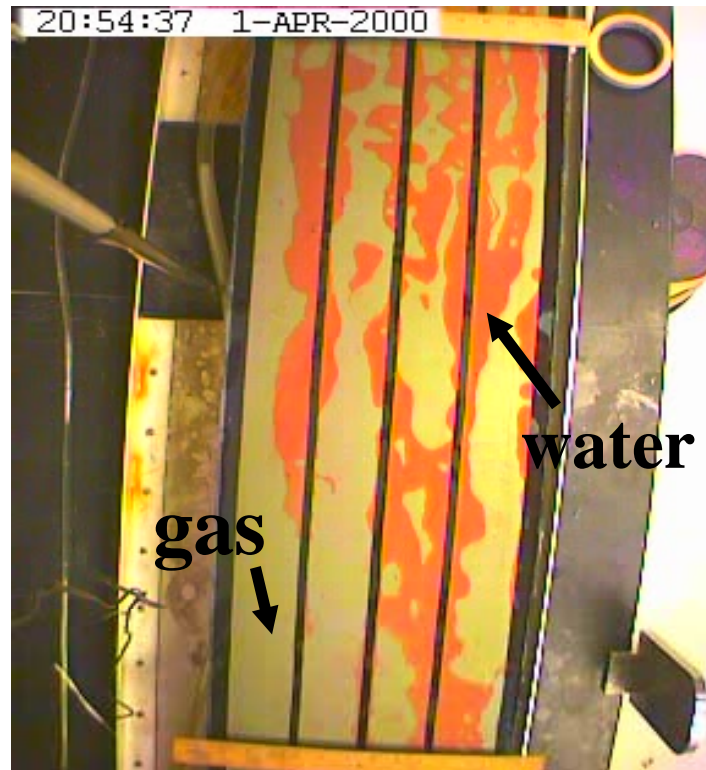
Figure 6.3 Sample camera image for two-phase run

Saturation was computed by measuring the area that each phase occupied. This was done by taking digital photographs of a constant area of the plate at a particular gas and water rate. The area is around 3 ft. long. This area was chosen far enough from the ends of the plates to prevent end effects. Figure 6.3 shows a sample photo of a two-phase run. The photographs were processed in a Matlab program.   The program uses quadratic discriminant analysis to group the pixels of the photograph into three groups: the water phase, gas phase and the shim. The grouping was based on color differences. Saturation was calculated as total pixels of liquid group over the sum of the gas and liquid group. Figure 6.4 is a comparison of the gray-scale image produce by the program and the original photograph from the digital camera. The accuracy of the program in calculating the saturation can be related to the similarity in details of the gray scale image to the true image. From the figure, it can be said that the program has reasonable accuracy.
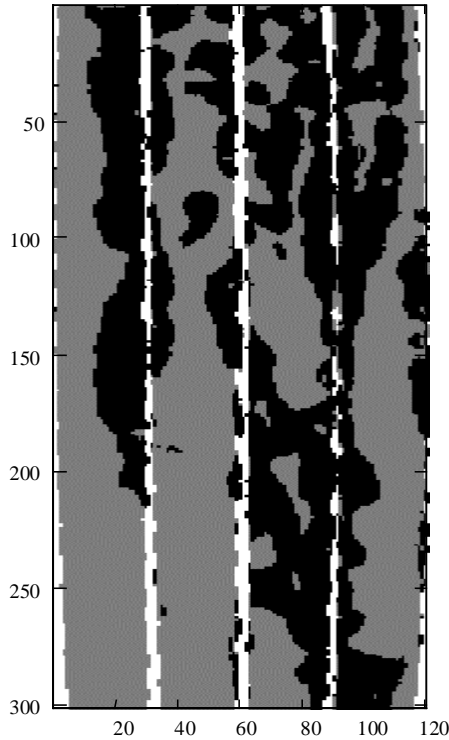
Saturation = 0.5987
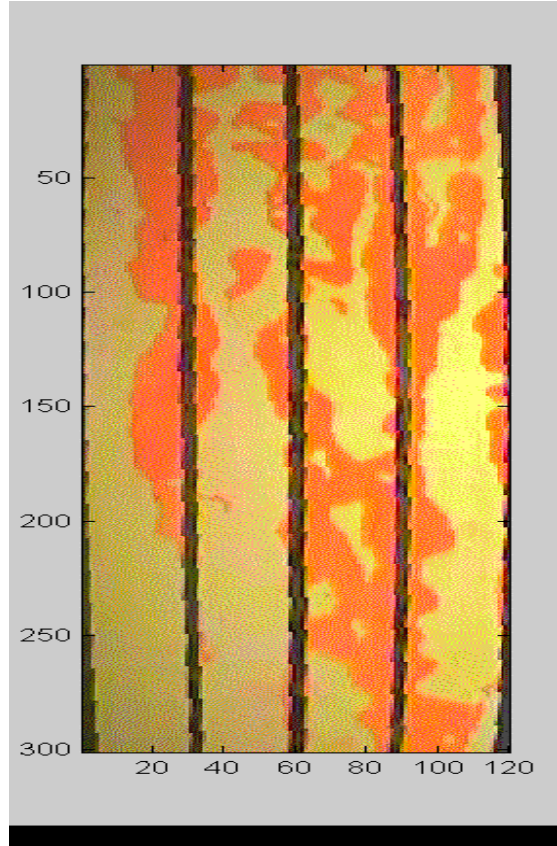
Figure 6.4 Comparison of gray-scale image produced by Matlab program to actual photo taken by digital camera.

Pan et al. (1996) also used this technique for measurement of saturation. Their study noted that the sources of error in this technique were the quality of the photographs and the water film adsorbed on the surfaces of the plates with the latter being of minimal effect. Good quality photographs are the ones with clear distinction between the gas and liquid phases. The use of dyed liquid enhanced visualization of phase boundaries and produced quality photographs.

6.2 PARTIAL RESULTS AND DISCUSSION

Preliminary experiments were done with q_{gas}/q_{liq} values of 1, 5, 10, 20 and single-phase runs at residual saturation. There were some important observations:

In these ratios of q_{gas}/q_{liq}, the water and gas phase travel along the plate as separate channels. These separate flow paths change with time and position. This is illustrated in the series of images in Figure 6.5, which were taken at constant gas and liquid rate. This observation imply that at these ratio, phases move individually and not as "moving islands" or "globules" of the discontinuous phase carried along by the other phase. It also suggests that there is no local steady-state saturation.
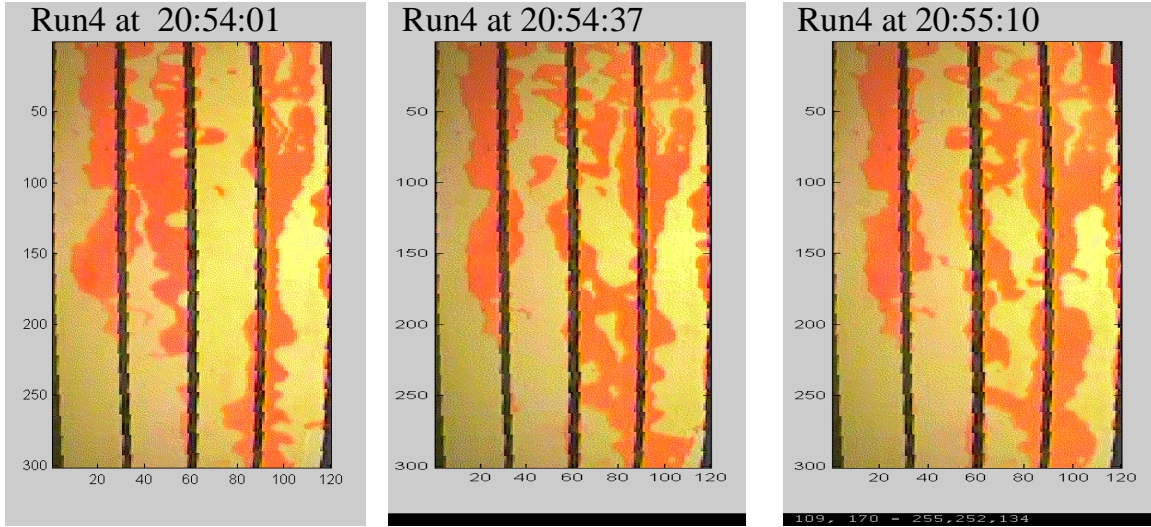
Figure 6.5 Images at constant gas and liquid rate in short time intervals to illustrate changes in the gas and liquid flow paths

These fast changes in flow paths are accompanied by pressure fluctuations. When the gas has established sufficient energy to break through the water flow path, there is a corresponding increase in inlet gas pressure and decrease in water line pressure. The same is true when the water phase breaches through gas channels. This has caused difficulty in observation since the pressure changes suddenly at these times.

Residual saturations obtained were very low. S_{wr} is around 0.02 -0.06 and S_{gr} is around 0.04-0.06. This indicates that there was negligible trapping in this smooth-walled fracture.

Pan et al. (1996) discussed two approaches in data analysis: the porous medium approach where Darcy's law is used and the homogeneous single-phase approach where the system is treated as a single-phase pipe flow. Because of the observations in the experiments, it seemed appropriate to treat the data using porous medium approach.

Darcy's law was used to obtained the single-phase and two-phase liquid permeability:

$$k_l = \frac{q_i \mu L}{(p_i - p_o)} \tag{6.1}$$

subscripts 'o' stands for outlet and 'i' for inlet, μ the viscosity, p as pressure, L for length of the plate and q as Darcy flow velocity from

$$q_o = \frac{Q_o}{bw} \tag{6.2}$$

where Q is the volumetric rate, b the aperture and w as the width of the plate.

The relative permeability is calculated by taking the ratio of the two-phase k_l with the single-phase k_l.

The gas permeability was calculated using the equation from Scheidegger (1974):

$$k_g = 2q_o \mu L \frac{p_o}{p_i^2 - p_o^2} \hspace{4cm} (6.3)$$

Similarly, taking the ratio of the two-phase k_g with single-phase run gives the relative permeability.

The complete list of calculated relative permeability values, their corresponding saturation range is shown in Table 6.1. Figure 6.6 and 6.7 shows the plot of these data along with the X-curves. The data is clustered at small saturation range and lies far from the X-curves. New experiments to extend the range of saturation values are planned for the near future.
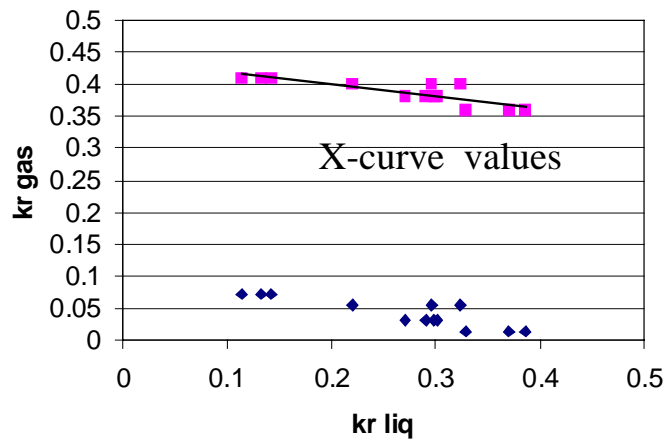
Figure 6.6 Comparison of experimental relative permeability values with X-curve values
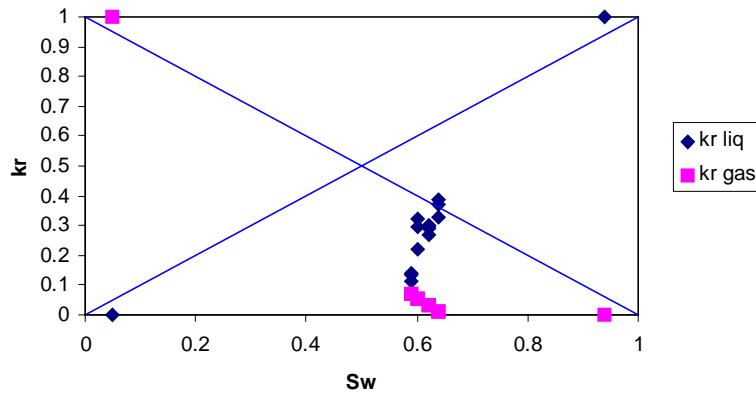
Figure 6.7 Experimental relative permeability values against saturation

6.2 DESIGN OF STEAM-WATER APPARATUS

The general technique used in the design for steam water apparatus is to pattern it after the current nitrogen-water system. The issues faced in the design are gaining accurate measurement of steam, water inlet and outlet flow, instantaneous saturation and pressure measurement, confinement of high steam pressure, maintaining good isothermal condition and prevention of leaks. With these many issues and uncertainty as to

experimental results, the main steam-water fracture apparatus was designed in a way to be flexible to future changes.

The process flow diagram for the experiment is shown in Fig. 6.6. In this experiment, steam and water will flow separately into the fracture. The apparatus will be kept at constant temperature. The two-phase outlet stream will be separated in a condenser.
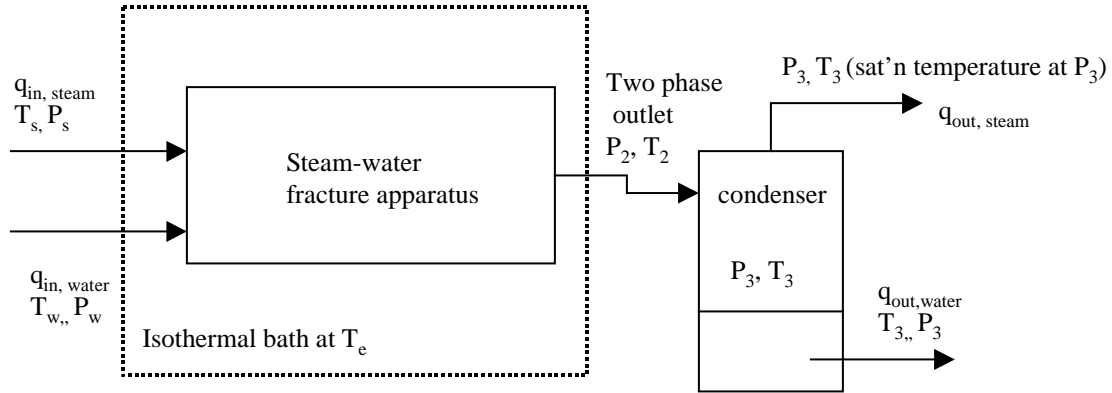
Figure 6.8 Process Schematic for Steam-Water Experiment

Isothermal conditions will be maintained by putting the whole fracture apparatus in a constant temperature air bath. Mirrors will be placed in the oven to reflect the image of the flow towards a video camera. The video will be used to measure saturation and to study the flow mechanism.

The fracture configuration will be maintained as a glass plate on top of an aluminum plate, with an o-ring placed between the glass and aluminum plate as a seal. The whole apparatus will be confined by a metal frame bolted to the bottom plate. This will improve the seal and to prevent deformation of the glass due to system pressure. The metal frame will have a window for flow visualization. (See Figure 6.9)

Top view

bolts
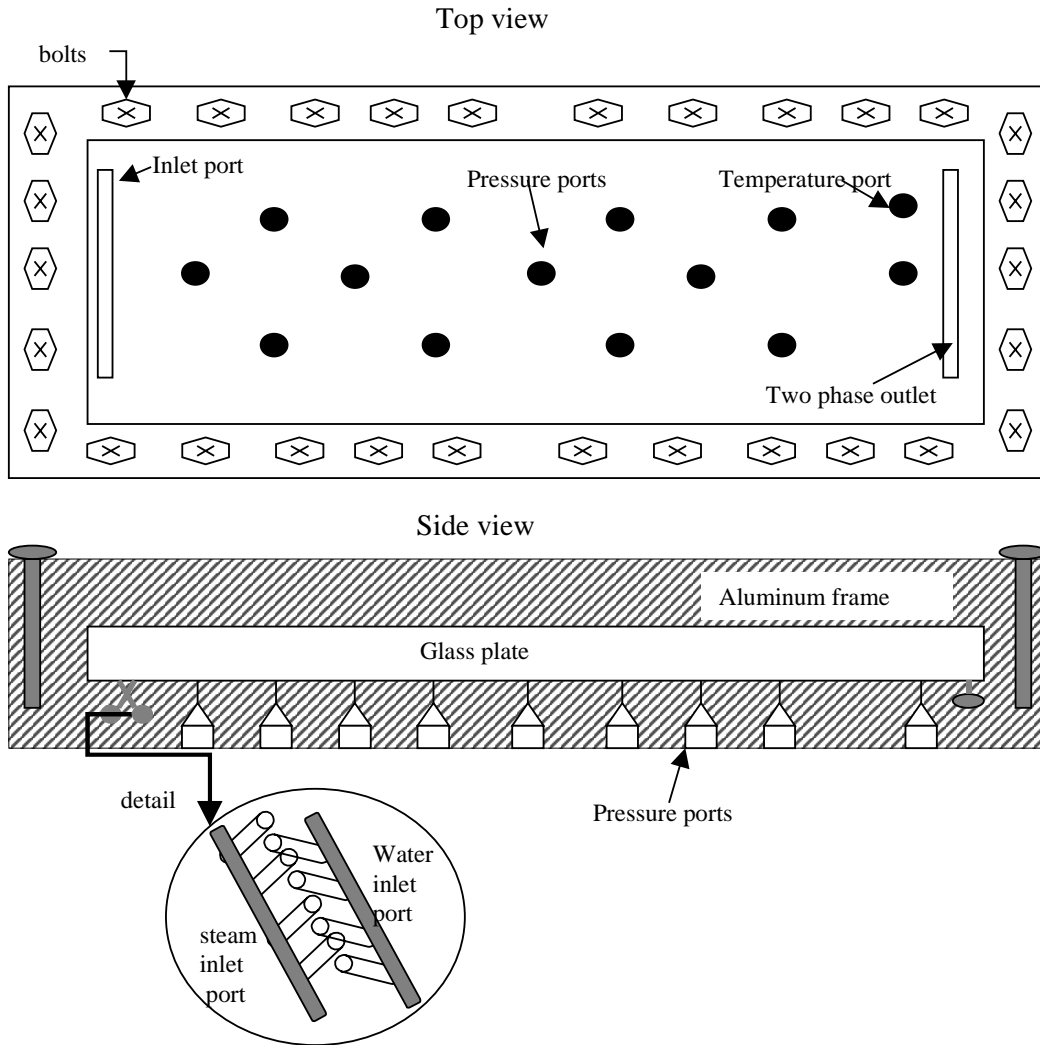
Figure 6.9 Schematic of steam-water fracture apparatus

Steam and water will enter the fracture through two separate channels. Each channel will have several ports drilled in a way that they align on the surface (See Figure 6.9). Throughout the flow area, tiny pressure ports the size of needles will be drilled. Needle size ports will minimize the surface discontinuity. One temperature port will be drilled at one end.

The fracture apparatus has been designed such that there is an available 12" by 4" space for flow. These dimensions were derived with the use of Equations 6.1 and 6.3. Given a set of relative permeability values, the equations were used to estimate pressure drop for different apparatus length and width. With the calculated pressure drop, an estimate for the condensation rate of the steam and evaporation rate of the water phase is made. The dimensions were chosen so as to have minimum condensation, evaporation and system pressure.

The amount of steam that will condense through the apparatus is proportional to the heat lost. Heat lost (Q_{lost}) is due to the temperature difference between the entering steam (T_s) and surrounding temperature (T_e).

$$Q_{lost} = kA\frac{dT}{dx} \approx klw(T_s - T_e)/h \qquad (6.4)$$

where k is the thermal conductivity of the glass, l, w and h are the length, width and height of the apparatus respectively.

The condensation rate is estimated by:

$$q_{condensation} = Q_{lost}/\Delta H_v \qquad (6.5)$$

where ΔH_v is the latent heat of vaporization at T_s.

The amount of water that will vaporize is related to the drop in pressure as water flows from p_w to p_2 (Figure 6.8). Energy balance gives:

$$x = \frac{(H_{sat'd\_water\_at\_Pw} - H_{sat'd\_water\_at\_P2})}{(H_{sat'd\_vapor\_at\_P2} - H_{sat'd\_water\_at\_P2})} \qquad (6.6)$$

where x is the weight fraction of steam, H represents enthalpy.

The glass plate will be 1" thick. The thickness of the glass plate was calculated through Equation 6.7, to have a conservative estimate for minimizing buckling or glass deformation.

$$\Delta y_{max} = \frac{wl^4}{384EI} \qquad (6.7)$$

where Δy_{max} represents the deformation of the glass vertically, E is the modulus of elasticity of the glass and I as the second moment of inertia equal to

$$I = \frac{lh^3}{12} \qquad (6.8)$$

6.3 FUTURE WORK

Further experiments with nitrogen-water system will be done at higher order of variation of q_{gas}/q_{liq}. This is to obtain wider saturation range in the relative permeability values and to further investigate the flow mechanism. The experiment will also be done with sand or glass beads in between the glass and aluminum plate to simulate flow through rough-walled fractures. Steam-water experiment with the new apparatus will also be conducted.

Table 6.1 Calculated Relative Permeability Values

run #	Qg	Gas Head	krg	Qw	Water Head	krl
	(cc/min)	(cm H2O)		(cc/min)	(cm H2O)	
1	74	12.5	0.013	35.16	11.5	0.385
1	74	12.5	0.013	33.77	11.5	0.370
1	74	12.5	0.013	29.97	11.5	0.328
2	172	13	0.030	26.51	11.5	0.291
2	172	13	0.030	27.45	11.5	0.301
2	172	13	0.030	27.19	11.5	0.298
3	172	13	0.030	24.71	11.5	0.271
3	332	13.7	0.055	26.98	11.5	0.296
3	332	13.7	0.055	29.51	11.5	0.323
3	332	13.7	0.055	20.04	11.5	0.220
4	407	12.8	0.072	12.36	11.0	0.142
4	407	12.8	0.072	9.92	11.0	0.114
4	407	12.8	0.072	11.52	11.0	0.132

7. REFERENCES

Ambusso, W., Satik, C., and Horne, R.N.: "Determination of Relative Permeability for Steam-Water Flow in Porous Media," paper SPE 36682, presented at the 1996 Annual Technical Conference and Exhibition, Denver, Colorado, Oct. 6-9.

Amyx, J.W., Bass, D.M., JR., and Whiting, R.L.: *Petroleum Reservoir Engineering-Physical Properties*, (1960), McGraw Hill Book Co., ISBN 07-001600-3, 92.

Anderson, A.W. and Gast, A.P.: "Physical Chemistry of Surface," 6th Edition, A Wiley-Interscience Publication, John Wilery & Sons, New York, 1997

Counsil, J.R.: "Steam-Water Relative Permeability," Ph.D. Dissertation, Stanford University (1979).

Ertekin, T., King, G.R., and Schwerer, F.C.: "Dynamic Gas Slippage: A Unique Dual-Mechanism Approach to the Flow of Gas in Tight Formation," paper SPE 12045, presented at the 1983 Annual Technical Conference and Exhibition, San Francisco, California, Oct. 5-8, 1983.

Estes, R.K. and Fulton, P.F.: "Gas Slippage and Permeability Measurements," *Trans.*, AIME, (1956), **207**, 338-342.

Fort, F.T.: "Implementation of West Panhandle Vacuum Operations," paper SPE 24297, presented at the 1992 SPE Mid-Continent Gas Symposium, Amarillo, Texas, April 13-14, 1992.

Fulton, P.F.: "The Effect of Gas Slippage on Relative Permeability Measurements," Producers Monthly (Oct., 1951), **15**, No. 12, 14.

Handy, L.L.: "Determination of Effective Capillary Pressures for Porous Media from Imbition Data," Petroleum Transactions AIME (1960), Vol. 219, 75-80.

Hanselman, D. and Littlefield, B. *Mastering Matlab 5 A Comprehensive Tutorial and Reference*, Prentice-Hall, Inc.,New Jersey, 1998.

Herkelrath, W.N., Moench, A.F., and O'Neal II, C.F.: "Laboratory Investigations of Steam Flow in a Porous Medium," *Water Resources Research* (August 1983), **19**, No.4, 931-937.

Horne, R.N., Satik, C., Mahiya, G., Li, K., Ambusso, W., Tovar, R., Wang, C., and Nassori, H.: "Steam-Water Relative Permeability," Proc. of the World Geothermal Congress 2000, Kyushu-Tohoku, Japan, May 28-June 10, 2000.

Horne, R.N., Ramey, H.J. Jr., Shang, S., Correa, A., and Hornbrook, J.: "The Effects of Adsorption and Desorption on Production and Reinjection in Vapor-Dominated Geothermal Fields," *Proc.* of the World Geothermal Congress, 1995, Florence, Italy, May, 1995, 1973-1977.

Jolly, R.J.H., Wei,L., Pine, R.J.,: "Stress Sensitive Fracture-Flow Modelling in Fractured Reservoirs," SPE 59042 (2000).

Jones, S.C., Roszelle, W.O.: "Graphical Techniques for Determining Relative Permeability From Displacement Experiments," SPE 6045 (1978).

Jones, F.O.: "A Laboratory Study of the Effects of Confining Pressure on Fracture Flow and Storage Capacity in Carbonate Rocks," SPE 4569.

Jones, F.O. and Owens, W.W.: "A Laboratory Study of Low-Permeability Gas Sands," *JPT* (September 1980), 1631-1640.

Klinkenberg, L.J.: "The Permeability of Porous Media to Liquids and Gases," *API Drilling And Production Practice* (1941), 200-213.

Li, K. and Horne, R.N.: "Characterization of Spontaneous Water Imbibition into Gas-Saturated Rocks," SPE 62552, presented at the 2000 SPE/AAPG Western Regional Meeting, Long Beach, California, 19–23 June 2000.

Li, K. and Horne R.N.: "Steam-Water Capillary Pressure in Geothermal Systems," *Proc.* of 25th Workshop on Geothermal Engineering, Stanford, CA, Jan. 24-26, 2000.

Li, K. and Horne R.N.: "Differences between Steam-Water and Air-Water Capillary Pressures," *Proc.* of 26th Workshop on Geothermal Engineering, Stanford, CA, Jan. 29-31, 2001.

Mahiya, G.F.: "Experimental Measurement of Steam-Water Relative Permeability," MS report, Stanford University, Stanford, CA, USA, 1999.

Pan, X., Wong, R.C., and Maini, B.B.: Steady State Two-Phase Flow in a Smooth Parallel Fracture, presented at the 47th Annual Technical Meeting of the Petroleum Society in Calgary, Alberta, Canada, June 10-12, 1996.

Persoff, P. and Hulen, J.B.: "Hydrologic Characterization of Four Cores from the Geysers Coring Project," *Proc.* of 21st Workshop on Geothermal Engineering, Stanford, CA, 1996.

Persoff, P., and Pruess, K.: Two-Phase Flow Visualization and Relative Permeability Measurement in Transparent Replicas of Rough-Walled Fractures, Proceedings, 16th Workshop on Geothermal Reservoir Engineering, Stanford University, Stanford, CA, Jan. 23-25, 1991, pp 203-210.

Pruess, K., and Tsang, Y. W.: On Two-Phase Relative Permeability and Capillary Pressure of Rough-Walled Rock Fractures, Water Resources Research 26 (9), (1990), pp 1915-1926.

Sampath, K. and Keighin, C.W.: "Factors Affecting Gas Slippage in Tight Sandstones of Cretaceous Age in the Uinta Basin," *JPT*, (November 1982), 2715-2720.

Satik, C. and Horne, R.N.: "Measurement of Steam-Water Relative Permeability," Quarterly report of Stanford Geothermal Program (January –March 1998), DE-FG07-95ID13370.

Scheidegger, A.E. *The Physics of Flow Through Porous Media*, 3rd ed., University of Toronto, Toronto. 1974.

Sta. Maria, R.B. and Pingol, A.S.: "Simulation the effects of Adsorption and Capillary Forces in Geothermal reservoirs," *Proc.* of 21st Workshop on Geothermal Engineering, Stanford, CA, 1996.

Stegemeier, G.L. and Vinegar, H.J.: "Soil Remediation by Surface Heating and Vacuum Extraction," paper SPE 29771, presented at the 1992 SPE/EPA Exploration & Production Environmental Conference, Houston, Texas, March 27-29, 1992.

Rose, W.D.: "Permeability and Gas-Slippage Phenomena,", 28th Annual Mtg. Topical Committee on Production Technology (1948).

Rose, W.D.: "Permeability and Gas-Slippage Phenomena," *API Drilling And Production Practice* (1948), 209.

Vinegar, H.J., Menotti, J.L., Coles, J.M., Stegemeier, G.L., Sheldon, R.B., and Edelstein, W.A.: "Remediation of Deep Soil Contamination Using Thermal Vacuum Wells," paper SPE 39291, presented at the 1997 SPE Annual Technical Conference and Exhibition, San Antonio, Texas, Oct. 5-8, 1997.

Wel, K.K., Morrow, N.R., and Brower, K.R.: "Effect of Fluid, Confining Pressure, and Temperature on Absolute Permeabilities of Low-Permeability Sandstones," *SPE Formation Evaluation* (August 1986), 413-423.